Stress Relaxation of Near-Critical Gels

Kurt Broderix*, Timo Aspelmeier, Alexander K. Hartmann and Annette Zippelius
Institute for Theoretical Physics, University of Göttingen, Bunsenstr. 9, 37073 Göttingen, Germany
(November 23, 2000)

The time-dependent stress relaxation for a Rouse model of a crosslinked polymer melt is completely determined by the spectrum of eigenvalues of the connectivity matrix. The latter has been computed analytically for a mean-field distribution of crosslinks. It shows a Lifshitz tail for small eigenvalues and all concentrations below the percolation threshold, giving rise to a stretched exponential decay of the stress relaxation function in the sol phase. At the critical point the density of states is finite for small eigenvalues, resulting in a logarithmic divergence of the viscosity and an algebraic decay of the stress relaxation function. Numerical diagonalisation of the connectivity matrix supports the analytical findings and has furthermore been applied to cluster statistics corresponding to random bond percolation in two and three dimensions.

I. INTRODUCTION

The most striking observation in near critical gels is the anomalous stress relaxation[1], which precedes the transformation of the viscous fluid into an elastic amorphous solid, i.e. the gelation transition. Here, polymer systems are considered, where the viscoelastic behavior is controlled by the concentration c of crosslinks connecting monomers of different molecules. At a critical concentration c_{crit} the gelation transition occurs. Viscoelastic studies by several groups have revealed the following characteristic features of stress relaxation:

- In the sol phase, well below the gelation transition, one observes a stretched exponential decay of the stress relaxation function $\chi(t) \sim \exp -(t/\tau^*)^\beta$.
- The time scale $\tau^* \sim \epsilon^{-z}$ diverges as the critical point is approached. Here $\epsilon = (c_{\text{crit}} - c)/c_{\text{crit}}$ denotes the distance from the critical point.
- The viscosity η, which is given as the integral over the stress relaxation function, diverges $\eta \sim \epsilon^{-k}$ as the critical point is approached.
- At the critical point, stress relaxation is algebraic in time: $\chi(t) \sim t^{-\Delta}$.

Whereas the stretched exponential decay is characteristic of the sol phase and holds for all crosslink concentrations $c < c_{\text{crit}}$, the last three observations refer to critical behavior, as the gel point is approached. If dynamic scaling holds, these findings can be cast in a scaling ansatz for the stress relaxation function $\chi(\epsilon, t)$, which depends on time and distance from the critical point ϵ:

$$\chi(c,t) = \epsilon^{z-k} g(t/\tau^*(\epsilon)) \tag{1}$$

with $\tau^* \sim \epsilon^{-z}$. Given a certain distance ϵ from the gel point, one expects to see a crossover from an algebraic decay at intermediate times to a stretched exponential decay at asymptotically large times. The scaling ansatz implies $\Delta = (z-k)/z$. Dynamic scaling as implied by Eq. (1) is well confirmed experimentally[2] for the intermediate time regime where $\chi(t)$ decays like a power law. However, the values for the exponents scatter considerably. Martin et al.[3] and Adolf et al.[2] find $\Delta = 0.7 \pm 0.05$ in agreement with the value $\Delta = 0.7 \pm 0.02$ of Durand et al.[4], whereas Winter and coworkers[5] observe a wide range of exponent values $0.2 \leq \Delta \leq 0.9$, depending on molecular weight and stoichiometry. The experimental support for a universal stretched exponential law is weak. Whereas Martin et al. confirm the stretched exponential decay and quote $\beta \sim 0.4$[3], other studies reveal non-universal exponents β. The divergence of the time scale $\tau^* \sim \epsilon^{-z}$ in the scaling function was determined in viscoelastic measurements as $z = 3.9 \pm 0.2$[3,2] and deduced from static measurements of the shear modulus as $z = 4.0 \pm 0.6$[6]. The experimental values for k, the

---

*deceased (2 May 2000)

critical exponent of the viscosity, vary in the range $0.7 \leq k \leq 1.4$. The origin of the scatter in the experimental data is not clear. One possible explanation is the size of the critical region, which is known to depend on the degree of polymerization. Hence experiments with different samples have to cope with different sizes of the critical region and possibly strong crossover effects.

In this paper we study the simplest dynamic model – Rouse dynamics – in the presence of a time dependent shear flow by means of analytical calculations and numerical simulations. Within this model, the frequency dependent stress relaxation is completely determined by the spectral properties of the connectivity matrix Γ, which specifies which monomers are crosslinked. As a function of the total concentration of crosslinks c one observes in general a percolation transition at a critical concentration c_{crit}, such that for $c < c_{\text{crit}}$ no macroscopic cluster of connected particles exist, whereas for $c > c_{\text{crit}}$ the system percolates. In the context of gelation the fraction of sites in the macroscopic cluster has been identified with the gel fraction and the percolation transition has been shown to mark the onset of solidification[7].

The connectivity matrix Γ is a positive semidefinite, random matrix, which has been studied in various contexts, e.g. diluted ferromagnets, diffusion in sparsely connected spaces[8], anomalous relaxation in glassy systems and localization[9]. In all cases the system consists of N vertices (monomers in the context of gelation) which are connected by cN edges (crosslinks). In the simplest case (mean field) one chooses the edges independently out of all possible $N(N-1)/2$ edges. The density of eigenvalues can be computed analytically for the above simple distribution and has been discussed in Refs. 8, 9 in the percolating regime, i.e. $c \geq c_{\text{crit}}$. In this paper we focus on the range $c \leq c_{\text{crit}}$, which corresponds to the sol phase and the critical point. For crosslinks of unit strength the spectrum of Γ is shown to consist of δ-functions only. For fluctuating crosslink strength, the spectrum is smooth and shows a Lifshitz tail for small eigenvalues. The spectrum determines the time dependent stress relaxation function of Eq. (1). In mean field theory the exponents are found to be $\beta = 1/3, \Delta = 1$ and $z = 3$. These results have been confirmed by numerical diagonalisation of the connectivity matrix Γ.

The latter approach can be extended to finite dimensional connectivities, corresponding to two and three dimensional percolation. Qualitatively the results are similar to mean-field theory with, however different exponent values. In $d = 2$ we find $\Delta \approx 0.74$ and $k \approx 1.19$. The latter value is in good agreement with a scaling relation, which was derived previously[10] and yields $k \sim 1.17$ using high precision data for the conductivity exponent[11]. Our numerical analyis in $d = 3$ is restricted to rather small system sizes ($\leq 20^3$) as compared to high precision data of Gingold et al.[12], because these authors restrict their investigations to the conductance, whereas we aim at the density of states, which requires a much larger numerical effort. Consequently our exponent values are of relatively low precision as compared to Ref. 12. Specifically we find $\Delta \approx 0.83$ and $k \approx 0.75$, whereas scaling together with high precision data yield for the latter $k \sim 0.71$.

The paper is organised as follows: In the following section (Sec. II) we introduce the dynamic model and the observables which we want to discuss and which can be related to the spectrum of eigenvalues of the connectivity matrix. In Sec. III we present the analytical calculations for the mean-field distribution of crosslinks. We briefly review the derivation of a selfconsistent equation for the spectrum, which was previously given by Bray and Rodgers[8]. We then go on to discuss the appearance of Lifshitz tails for small eigenvalues. For crosslinks of unit strength the spectrum is shown to consist of a countable set of δ-peaks. We present an analytical scheme to systematically compute the spectrum by iteration. We also consider crosslinks of fluctuating stength, for which the spectrum is continuous and can be obtained by standard numerical means from the selfconsistent integral equation. In Sec. IV we present results from a numerical diagonalisation of random connectivity matrices. We first compute the spectrum for a mean-field distribution of crosslinks and compare it to the analytical results. Next, cluster distributions of random bond percolation in 2 and 3 dimensions are considered. Data for the stress relaxation function is presented as well as finite size scaling plots for the static shear viscosity. We summarize our results in Sec. V. Some detailed calculations have been deferred to appendices.

Our paper is an extension of previous work, in which we discussed the static shear viscosity[10,13] and self diffusion[14] in the sol phase as well as at the gelation transition. There it was shown that the long time limit of the incoherent scattering function is determined by the zero eigenvalues of the connectivity matrix, and the static shear viscosity is determined by the trace of the Moore-Penrose inverse of the connectivity matrix. Here we focus on the *full* spectrum of eigenvalues, which also determines the decay of the stress relaxation at *finite* times.

II. MODEL AND OBSERVABLES

We consider a system of N identical Brownian particles, each characterized by its time-dependent position vector $\mathbf{R}_i(t)$ $(i = 1, \dots, N)$ in d-dimensional space of volume V, i.e. with density $\rho = N/V$. M permanent crosslinks are introduced between randomly chosen pairs of particles (i_e, i'_e), resulting in a crosslink concentration $c = M/N$. These crosslinks are modelled by a harmonic potential

$$U := \frac{d}{2a^2} \sum_{e=1}^{M} \lambda_e \big(\mathbf{R}_{i_e} - \mathbf{R}_{i'_e}\big)^2, \tag{2}$$

whose overall strength is controlled by the parameter $a > 0$. We use units of energy such that $k_{\mathrm{B}}T = 1$ and allow for fluctuations in the strength of crosslinks by introducing the parameter λ_e. Crosslinks of uniform strength correspond to all $\lambda_e = 1$. In general each crosslink e is assigned independently a random strength λ_e according to the distribution $p(\lambda)$. The connectivity of the particles is specified by the connectivity matrix

$$\Gamma_{ii'} = \sum_{e=1}^{M} \lambda_e (\delta_{ii_e} - \delta_{ii'_e})(\delta_{i'i_e} - \delta_{i'i'_e}), \tag{3}$$

in terms of which the potential reads $U = (d/2a^2) \sum_{i,i'=1}^{N} \Gamma_{ii'}\, \mathbf{R}_i \cdot \mathbf{R}_{i'}$. As usual δ_{ij} denotes the Kronecker symbol, i.e. $\delta_{ij} = 1$ for $i = j$ and zero otherwise.

We consider purely relaxational dynamics in an externally applied space- and time-dependent velocity field $v^{\alpha}_{\mathrm{ext}}(\mathbf{r}, t)$:

$$\partial_t R_i^{\alpha}(t) = -\frac{1}{\zeta} \frac{\partial U}{\partial R_i^{\alpha}}(t) + v^{\alpha}_{\mathrm{ext}}\big(\mathbf{R}_i(t), t\big) + \xi_i^{\alpha}(t). \tag{4}$$

Here, Greek indices indicate Cartesian co-ordinates $\alpha = x, y, z, \ldots$, and we will always consider a flow field in the x-direction, increasing linearly with y, *i.e.*

$$v^{\alpha}_{\mathrm{ext}}(\mathbf{r}, t) = \delta_{\alpha,x} \kappa(t) r_y, \tag{5}$$

with a time-dependent shear rate $\kappa(t)$. The noise $\boldsymbol{\xi}$ has zero mean and covariance $\langle \xi_i^{\alpha}(t)\, \xi_{i'}^{\beta}(t') \rangle = 2\zeta^{-1}\, \delta_{\alpha,\beta}\, \delta_{i,i'}\, \delta(t-t')$, where $\delta(t)$ is the Dirac δ-function. Here, the bracket $\langle \cdots \rangle$ indicates the average over the realizations of the Gaussian noise $\boldsymbol{\xi}$. The relaxation constant is denoted by ζ. The probability distribution of crosslink configurations $\mathcal{G} = \{i_e, i'_e\}_{e=1}^{M}$ as well as the probability distribution of crosslink strengths will be specified later.

In Ref. 10 we have computed the shear viscosity in the sol phase for (macro-) molecular units of arbitrary internal connectivity. It was shown that the dependence on the crosslink concentration and in particular the critical behavior near the gelation threshold is the same for all (macro-) molecular units, as long as we consider identical units with a finite degree of polymerization. We expect the same universal behavior for stress relaxation on long time scales, which are much larger than the longest internal time scale of a single (macro-) molecule. Hence we specialize to the simplest units, namely Brownian particles.

Relaxation of shear stress

We aim at the computation of the intrinsic shear stress $\sigma_{\alpha\beta}(t)$ as a function of the shear rate $\kappa(t)$. For the simple shear flow (5), a linear response relation

$$\sigma_{xy}(t) = \int_{-\infty}^{t} \mathrm{d}\tau\, \chi(t-\tau)\kappa(\tau) \tag{6}$$

is valid for arbitrary strengths of the shear rate $\kappa(t)$. The linear response or shear relaxation function $\chi(t)$ is given in terms of the connectivity matrix as explained in detail in Ref. 13

$$\chi(t) = \frac{\rho}{N} \sum_{i=1}^{N} \left((1 - E_0(\mathcal{G})) \exp\left\{ -\frac{2dt}{\zeta a^2} \Gamma(\mathcal{G}) \right\} \right)_{ii} =: \frac{\rho}{N} \operatorname{Tr} \left((1 - E_0(\mathcal{G})) \exp\left\{ -\frac{2dt}{\zeta a^2} \Gamma(\mathcal{G}) \right\} \right). \tag{7}$$

The matrix E_0 denotes the projector onto the subspace of zero eigenvalues of Γ[10]. For a time independent shear rate, $\kappa(t) = \kappa$, the stress tensor is time independent and related to the shear rate $\sigma = \rho\eta\kappa$ via the static shear viscosity, given by[10]

$$\eta = \frac{\zeta a^2}{2dN} \operatorname{Tr} \frac{1 - E_0(\mathcal{G})}{\Gamma(\mathcal{G})}. \tag{8}$$

Selfdiffusion

To discuss selfdiffusion we set the externally applied velocity field to zero and focus on the incoherent scattering function

$$S(\mathbf{q},t) := \lim_{T\to\infty} \left\langle \frac{1}{N}\sum_{i=1}^{N} \exp\left\{ \mathrm{i}\,\mathbf{q}\left(\mathbf{R}_i(t+T)-\mathbf{R}_i(T)\right)\right\}\right\rangle \tag{9}$$

and the squared time delayed displacement

$$C(t) := \lim_{T\to\infty} \left\langle \frac{1}{N}\sum_{i=1}^{N} (\mathbf{R}_i(t+T)-\mathbf{R}_i(T))^2 \right\rangle . \tag{10}$$

We note that $\mathbf{R}_i(t+T)-\mathbf{R}_i(t)$ is a Gaussian Markov process whose distribution is in the limit $T\to\infty$ characterized by a vanishing mean and the covariance function

$$\begin{aligned} G_{ii'}(t) &:= \lim_{T\to\infty} \Big\langle [\mathbf{R}_i(t+T)-\mathbf{R}_i(T)]\,[\mathbf{R}_{i'}(t+T)-\mathbf{R}_{i'}(T)] \Big\rangle \\ &= \frac{1}{\zeta}\int_0^t \mathrm{d}\tau\, \left(\exp\left\{-\frac{2d\tau}{\zeta a^2}\Gamma\right\}\right)_{ii'} . \end{aligned} \tag{11}$$

Performing the integral in (11) leads to

$$G_{ii'}(t) = \frac{2}{\zeta}\left(\frac{\zeta a^2}{2d}\frac{1-E_0}{\Gamma}\,\left(1-\exp\left\{-\frac{2dt}{\zeta a^2}\Gamma\right\}\right) + t\,E_0\right)_{ii'} . \tag{12}$$

The matrix Γ is non-negative by inspection (see Eq. (2)), as it should be to ensure relaxation to equilibrium. The scattering function as well as the time delayed displacement can be expressed in terms of $G_{ii'}(t)$ via

$$S(\mathbf{q},t) = \frac{1}{N}\sum_{i=1}^{N} \exp\left\{-q^2\, G_{ii}(t)\right\} \tag{13}$$

and

$$C(t) = \frac{1}{N}\sum_{i=1}^{N} G_{ii}(t). \tag{14}$$

Density of eigenvalues

All dynamic quantities of interest have been expressed in terms of Γ. Accordingly, once we know the eigenvalues $\{\gamma_i\}_{i=1}^{N}$ and eigenvectors of this matrix, we can compute dynamic observables for arbitrary times. In the following, we shall discuss the density of eigenvalues

$$D_{\mathrm{tot}}(\gamma) = \lim_{N\to\infty} \overline{\frac{1}{N}\sum_{i=1}^{N}\delta(\gamma-\gamma_i)} = \lim_{N\to\infty} \overline{\frac{1}{N}\,\mathrm{Tr}\,\delta(\gamma-\Gamma)} \tag{15}$$

for several crosslink distributions. Here $\overline{\cdot}$ denotes the average over crosslink realizations. If one splits off the zero eigenvalues, $D_{\mathrm{tot}}(\gamma)$ can be written as

$$D_{\mathrm{tot}}(\gamma) = T_0(c)\delta(\gamma) + (1-T_0(c))D(\gamma). \tag{16}$$

where $D(\gamma)$ is normalized to 1 and contains only the non-zero eigenvalues. If we group the particles into clusters, the eigenspace of modes with zero eigenvalues corresponds to vectors that are constant within one cluster[14]. In other words there is one zero eigenvalue for each cluster and the dimension of the null space is just the number of clusters N_{cl}. The weight of zero eigenvalues is simply given by the density of clusters, i.e. $T_0(c) = N_{\mathrm{cl}}/N$.

We restrict ourselves to the density of eigenvalues and do not attempt to compute eigenvectors, which is in general more difficult. Hence we can only compute observables which can be written as $\frac{1}{N}\sum_{i=1}^{N}(f(\Gamma))_{ii}$, where f is an arbitrary function of Γ. The incoherent scattering function is not of this form (Eq. 13), whereas the stress relaxation function is

$$\overline{\chi(t)} = (1 - T_0(c))\rho \int_0^\infty \mathrm{d}\gamma D(\gamma) \exp\left\{-\frac{2dt}{\zeta a^2}\gamma\right\}. \tag{17}$$

The zero eigenvalues are not to be included in the integration, due to the term $1 - E_0$ in Eq. (7). Analogously, the averaged viscosity is given by

$$\overline{\eta} = (1 - T_0(c))\frac{\zeta a^2}{2d}\int_0^\infty \mathrm{d}\gamma \frac{D(\gamma)}{\gamma}. \tag{18}$$

In the same way, the disorder averaged, time delayed displacement is determined by

$$\overline{C(t)} = (1 - T_0(c))\frac{a^2}{d}\int_0^\infty \mathrm{d}\gamma \frac{D(\gamma)}{\gamma}\left(1 - \exp\left\{-\frac{2dt}{\zeta a^2}\gamma\right\}\right) + T_0(c)\frac{2t}{\zeta}. \tag{19}$$

It can also be expressed as an integral over the time dependent response function

$$\overline{C(t)} = \frac{2}{\zeta\rho}\int_0^t \mathrm{d}\tau\overline{\chi(\tau)} + T_0(c)\frac{2t}{\zeta}. \tag{20}$$

III. MEAN FIELD THEORY

We consider first the simplest distribution of crosslinks which ignores all correlations between crosslinks, i.e. the crosslinks are chosen independently of each other and each pair (i_e, i'_e) of particle indices is realized with equal probability. As shown in Ref. 15 the particle clusters exhibit the analog of a percolation transition at a critical crosslink concentration $c_{\mathrm{crit}} = 1/2$. Below this concentration there is no macroscopic cluster and almost all finite clusters are trees. The average number of tree clusters T_n with n particles is given in the macroscopic limit by

$$\lim_{N\to\infty}\frac{T_n}{N} = \tau_n = \frac{n^{n-2}(2c\,\mathrm{e}^{-2c})^n}{2c\,n!}. \tag{21}$$

In particular the total number of clusters per particle is

$$T_0(c) = 1 - c. \tag{22}$$

These results are independent of the distribution of crosslink strengths, $p(\lambda)$.

To compute the density of eigenvalues we introduce the resolvent

$$G(\Omega) = \lim_{N\to\infty}\frac{1}{N}\overline{\mathrm{Tr}\frac{1}{\Gamma - \Omega}} \tag{23}$$

for complex argument $\Omega = \gamma + i\epsilon, \epsilon > 0$. In the limit $\epsilon \to 0$, we recover the spectrum from the imaginary part of the resolvent according to

$$D_{\mathrm{tot}}(\gamma) = \frac{1}{\pi}\lim_{\epsilon\downarrow 0}\mathrm{Im}G(\gamma + i\epsilon). \tag{24}$$

It can be inferred from Eq. (15) that conversely, $D_{\mathrm{tot}}(\gamma)$ determines $G(\Omega)$ via

$$G(\Omega) = \int_{-\infty}^{\infty}\mathrm{d}\gamma\frac{D_{\mathrm{tot}}(\gamma)}{\gamma - \Omega}. \tag{25}$$

A. Disorder average by replicas

Bray and Rodgers[8] have shown how to reduce the computation of $D_{\rm tot}(\gamma)$ for crosslinks of unit strength (i.e. all $\lambda_e = 1$) to the solution of a nonlinear integral equation. Their derivation is easily generalized to crosslinks of strength λ which fluctuates according to a given distribution $p(\lambda)$. We restrict ourselves to distributions $p(\lambda)$ such that

$$\int_0^\infty \frac{\mathrm{d}\lambda}{\lambda}\, p(\lambda) < \infty \tag{26}$$

holds. It will be shown below (see Eq. (37)) that this condition is necessary to ensure a finite viscosity in the sol phase. Following Bray and Rodgers we introduce a generating function

$$Z(\Omega) = \int_{\mathbb{R}^N} \left(\prod_{i=1}^N \frac{d\phi_i}{\sqrt{2\pi}} \right) \exp\left(\frac{i}{2} \sum_{i,j} \phi_i \phi_j (\Omega \delta_{ij} - \Gamma_{ij}) \right), \tag{27}$$

which determines the resolvent, according to

$$G(\Omega) = \lim_{N\to\infty} \frac{2}{N} \overline{\frac{\partial \log Z}{\partial \Omega}}. \tag{28}$$

The average over the disorder is performed with the replica trick, resulting in

$$\overline{Z^n} = \int_{\mathbb{R}^N} \left(\prod_{i=1}^N \prod_{\alpha=1}^n \frac{d\phi_i^\alpha}{\sqrt{2\pi}} \right) \exp\left(\frac{i}{2} \Omega \sum_{i=1}^N \hat{\phi}_i \hat{\phi}_i + \frac{c}{N} \int_0^\infty d\lambda p(\lambda) \sum_{i,j=1}^N e^{-i\lambda(\hat{\phi}_i - \hat{\phi}_j)^2/2} - cN \right). \tag{29}$$

We assume that the connectivity is intensive, $\lim_{N\to\infty}(c/N) = 0$ and have introduced the notation $\hat{\phi}_i = (\phi_i^1, \phi_i^2, \ldots, \phi_i^n)$ for n-times replicated variables. In the next step one decouples different sites as shown in Ref. 8 and performs a saddle point approximation for large N. This gives rise to a self-consistent equation for a function $g^\Omega(\hat{x})$

$$g^\Omega(\hat{x}) = 2c \int_0^\infty d\lambda p(\lambda) \frac{\displaystyle\int d\hat{y} e^{(i\Omega \hat{y}^2 + 2g^\Omega(\hat{y}) - i\lambda(\hat{y}-\hat{x})^2)/2}}{\displaystyle\int d\hat{y} e^{(i\Omega\hat{y}^2 + 2g^\Omega(\hat{y}))/2}} \tag{30}$$

which in turn determines the resolvent according to

$$G(\Omega) = \lim_{n\to 0} \frac{i}{n} \frac{\displaystyle\int d\hat{x} \hat{x}^2 e^{(i\Omega\hat{x}^2/2 + g^\Omega(\hat{x}))}}{\displaystyle\int d\hat{x} e^{(i\Omega\hat{x}^2/2 + g^\Omega(\hat{x}))}}. \tag{31}$$

In the last step of the calculation one assumes a replica symmetric solution for the saddle point equation:

$$g^\Omega(\hat{x}) = g^\Omega(\rho) \text{ with } \rho = \sqrt{\sum_\alpha x_\alpha^2}. \tag{32}$$

The limit $n \to 0$ can then be performed resulting in the following nonlinear integral equation for $g^\Omega(\rho)$ (cf. Eqs. (16,17) in Ref. 8)

$$\begin{aligned} g^\Omega(\rho) &= 2c \int_0^\infty \mathrm{d}\lambda\, p(\lambda)\, \exp\left\{ -\frac{i\lambda}{2} \rho^2 \right\} \\ &\quad + 2ic\, e^{-2c} \int_0^\infty \mathrm{d}\lambda\, p(\lambda) \int_0^\infty \mathrm{d}x\, \lambda\rho\, \mathrm{I}_1(i\lambda\rho x)\, \exp\left\{ -\frac{i\lambda}{2}(\rho^2 + x^2) + \frac{i\Omega}{2} x^2 + g^\Omega(x) \right\} \end{aligned} \tag{33}$$

with $g^{\Omega}(0) = 2c$. Here $\mathrm{I}_\nu(z)$ are the modified Bessel functions of the first kind. The solution of Eq. (33) yields the resolvent

$$G(\Omega) = -\int_0^\infty \frac{\mathrm{d}\lambda}{\lambda}\, p(\lambda) + \frac{i}{2c}\int_0^\infty \mathrm{d}\rho\, \rho\, g^{\Omega}(\rho) \tag{34}$$

and the density of eigenvalues

$$D_{\mathrm{tot}}(\gamma) = \frac{1}{2c\pi}\lim_{\epsilon\to 0} \mathrm{Im}\left\{ i\int_0^\infty d\rho\rho g^{\gamma+i\epsilon}(\rho)\right\}. \tag{35}$$

B. Moments and Lifshitz tails

If all inverse moments M_n of the density of non-zero eigenvalues $M_n := \int_0^\infty \mathrm{d}\gamma\gamma^{-n} D(\gamma)$, $n \in \mathbb{N}$, exist, one can derive the following asymptotic expansion of the resolvent

$$G(\Omega) = \frac{c-1}{\Omega} + \frac{2d\eta}{\zeta a^2} + c\sum_{n=1}^{\infty} \Omega^n\, M_{n+1} \tag{36}$$

by expanding the denominator in Eq. (25) in a geometric series. As we show in Appendix A, the lowest moments are given explicitly by

$$M_1 = \frac{1}{4c}\left[\ln\left(\frac{1}{1-2c}\right) - 2c\right]\int_0^\infty \frac{\mathrm{d}\lambda}{\lambda}\, p(\lambda) = \frac{2d\eta}{\zeta a^2} \tag{37}$$

and

$$M_2 = -\frac{\left(5\,P_2 - 4\,P_1^2\right)}{240c^2}\ln\left(\frac{1}{1-2\,c}\right) - \frac{8\,c^3 - 6\,c^2 - 5\,c + 1}{30c\,(1-2\,c)^3}\,P_1^2 - \frac{4\,c^2 - 3\,c - 1}{24c\,(1-2\,c)^2}\,P_2 \tag{38}$$

with $P_n := \int_0^\infty \mathrm{d}\lambda\lambda^{-n}\, p(\lambda)$. Here and in the following we assume that very weak crosslinks are unlikely to occur, because we are interested in the small eigenvalues which are due to the geometry of the clusters and not due to the appearance of weak links. More precisely we require

$$\lim_{\lambda\downarrow 0} \frac{\ln|\ln p(\lambda)|}{|\ln\lambda|} > \frac{1}{2}. \tag{39}$$

The divergence of the moments, M_1 and M_2, suggests a Lifshitz tail of the density of states of the following form

$$D(\gamma) \propto \exp\left\{-\left(\frac{\gamma_0(1-2c)^3}{\gamma}\right)^{\kappa}\right\}, \quad \gamma\downarrow 0, \quad c < \tfrac{1}{2}, \tag{40}$$

since for positive κ, this ansatz implies for the inverse moments

$$M_n \propto (1-2c)^{-3(n-1)}, \quad c\uparrow \tfrac{1}{2}. \tag{41}$$

Bray and Rodgers have given a heuristic argument in favor of the ansatz (40) with $\kappa = 1/2$. They argue that out of all clusters for given n the linear one has the smallest eigenvalue, namely $\gamma_{\mathrm{min}} = \gamma_0 n^{-2}$. There is just one linear cluster for given n, so that its contribution to the spectrum is

$$D^{\mathrm{lin}} = \frac{1}{2c}\sum_n \left(2ce^{(-2c)}\right)^n \delta\left(\gamma - \frac{\gamma_0}{n^2}\right) \sim e^{-\sqrt{\gamma_0/\gamma}}. \tag{42}$$

Arbitrary finite clusters may be attached to the chain without altering the dependence of the smallest eigenvalue on the length of the chain. If a finite cluster of mass m_i is attached to site i of the linear chain, the smallest eigenvalue is $\gamma_{min} = \frac{\gamma_0}{m_i n^2}$. Replacing

$$m_i \sim \overline{m} = \frac{\sum_n n\tau_n}{\sum_n \tau_n} = \frac{1}{1-2c} \tag{43}$$

leads to $\gamma_{min} = \frac{\gamma_0(1-2c)}{n^2}$. The number of clusters contributing to $D(\gamma)$ for small γ is much larger, if attachments are taken into account: The probability to find a chain of length n, regardless of attachments, is given by $(2c)^n$. Hence the density of eigenvalues is estimated as

$$D^{\rm lin} = \frac{1}{2c}\sum_n (2c)^n \delta\left(\gamma - \frac{\gamma_0(1-2c)}{n^2}\right) \sim \exp\left\{-\left(\frac{\gamma_0(1-2c)^3}{\gamma}\right)^{1/2}\right\}. \tag{44}$$

Here, we have expanded $\ln(2c) \sim 2c - 1$ for c sufficiently close to its critical value $c_{crit} = 1/2$ to obtain the Lifshitz tail near criticality. In Appendix A.3 we derive rigorous upper and lower bounds for $D(\gamma)$, which prove that $D(\gamma)$ has indeed a Lifshitz tail of the form $D(\gamma) \sim \exp(-\sqrt{h(c)/\gamma})$. We are unable to derive the dependence of $h(c)$ on crosslink concentration c, which is however suggested by the lowest order moments (38),(74).

In the following two subsections we shall discuss two special choices for $p(\lambda)$. In the first case all crosslinks are of unit strength, giving rise to a point spectrum. In the second case the strength of the crosslinks fluctuates according to $p(\lambda) = \exp(-1/\lambda)/\lambda^2$. The integral equation (33) simplifies considerably for this distribution and allows for a solution by iteration.

C. Exact solution of the integral equation for uniform crosslink strengths

For crosslinks of unit strength, the integral equation (33) reduces to Eq. (16) in Ref. 8,

$$\begin{aligned} g^{\Omega}(\rho) &= 2c\exp\left(-\frac{i}{2}\rho^2\right)\left\{1 + i\,e^{-2c}\int_0^\infty {\rm d}x\,\rho\,{\rm I}_1(i\rho x)\,\exp\left(\frac{i(\Omega-1)}{2}x^2 + g^{\Omega}(x)\right)\right\} \\ &= 2c\exp\left(-\frac{i}{2}\rho^2\right)\left\{1 - 2c\,e^{-2c}\int_0^\infty {\rm d}x\,{\rm J}_1(x)\exp\left(\frac{i}{2}(\Omega-1)\frac{x^2}{\rho^2} + g^{\Omega}(\frac{x}{\rho})\right)\right\}. \end{aligned} \tag{45}$$

The second equality follows from a substitution $x \to \rho x$ and from the basic relation between the Bessel functions of the first kind ${\rm J}_\nu$ and the modified Bessel functions ${\rm I}_\nu$, in particular ${\rm I}_1(x) = -i\,{\rm J}_1(i\,x)$.

To get some feeling for the spectrum of eigenvalues, we first consider the case of small c. We then have predominantly small clusters, i.e. single particles, dimers, trimers etc. The connectivity matrix of a dimer has eigenvalues $\lambda_1 = 0, \lambda_2 = 2$. A linear chain of 3 particles has eigenvalues $\{0,1,3\}$, a linear chain of four particles has eigenvalues $\{0,2,2+\sqrt{2},2-\sqrt{2}\}$ and a star with three legs has eigenvalues $\{0,1,4\}$. These are the only trees up to $\mathcal{O}(c^3)$. Hence in this order the spectrum consists of δ-functions at the above eigenvalues, with each cluster contributing to the weight of the δ-functions according to its frequency of occurrence. Next we show that δ-functions in the spectrum correspond to Gaussian functions $g^{\Omega}(\rho)$. The ansatz

$$g^{\Omega}(\rho) = 2ca\exp\left(-i\,z(\Omega)\rho^2/2\right) \tag{46}$$

where $z = z(\Omega)$ is an arbitrary function of $\Omega = \gamma + i\epsilon$ with ${\rm Im}\{z\} < 0$ for $\epsilon > 0$, leads to $G(\Omega) = -1 + \frac{a}{z}$. In the limit ${\rm Im}\{z\} \to 0$ each zero γ_i of ${\rm Re}\{z(\gamma_i)\} = 0$ gives rise to a δ function in the spectrum

$$D_{\rm tot}(\gamma) = a\sum_i \frac{\delta(\gamma-\gamma_i)}{|\partial z/\partial\gamma(\gamma_i)|} \tag{47}$$

Next, we construct an approximation to the integral equation (45) by successive iteration. We start with

$$g_0^{\Omega}(\rho) := 2c. \tag{48}$$

The first step of the iteration gives

$$g_1^{\Omega}(\rho) = 2c\exp\left(-\frac{i}{2}\rho^2\right)\left\{1 - e^{-2c}\int_0^\infty dx\,{\rm J}_1(x)\exp\left(\frac{i}{2}(\Omega-1)\frac{x^2}{\rho^2} + g_0^{\Omega}(\frac{x}{\rho})\right)\right\} \tag{49}$$

$$= 2c\exp\left(-\frac{i}{2}\frac{\Omega}{\Omega-1}\rho^2\right) \tag{50}$$

since the integral on the rhs can be calculated exactly[16]. The spectrum consists of a δ-function at $\gamma = 0$, $D_1(\gamma) = \delta(\gamma)$. The next step of the iteration gives

$$g_2^\Omega(\rho) = 2c\exp\left(-\frac{i}{2}\rho^2\right)\left\{1 - e^{-2c}\int_0^\infty dx\, \mathrm{J}_1(x)\exp\left(\frac{i}{2}(\Omega-1)\frac{x^2}{\rho^2} + g_1^\Omega(\frac{x}{\rho})\right)\right\} \tag{51}$$

$$= 2c\exp\left(-\frac{i}{2}\rho^2\right)\left\{1 - e^{-2c}\int_0^\infty dx\, \mathrm{J}_1(x)\exp\left(\frac{i}{2}(\Omega-1)\frac{x^2}{\rho^2}\right)\sum_{k=0}^\infty \frac{(2c)^k}{k!}\exp\left(-\frac{i}{2}\frac{k\Omega}{\Omega-1}\frac{x^2}{\rho^2}\right)\right\} \tag{52}$$

by Taylor expansion of the exponential of $g_1^\Omega(\frac{x}{\rho})$. Again, the integrals appearing in Eq. (52) can be computed exactly, yielding

$$g_2^\Omega(\rho) = 2c\sum_{k=0}^\infty a_k^{(2)}\exp\left(-\frac{i}{2}z_k^{(2)}\rho^2\right) \tag{53}$$

$$a_k^{(2)} := e^{-2c}\frac{(2c)^k}{k!}, \quad z_k^{(2)} := (1 + \frac{1}{\Omega - 1 - k\frac{\Omega}{\Omega-1}}). \tag{54}$$

Note that $\sum_{k=0}^\infty a_k^{(2)} = 1$. In this iteration, the spectrum is given by

$$D_2(\gamma) = \frac{1-e^{-2c}}{2c}\delta(\gamma) + \sum_{k=2}^\infty e^{-2c}\frac{(2c)^{k-1}}{k(k-2)!}\delta(\gamma - k). \tag{55}$$

Next, we consider a general ansatz for g_i^Ω of the form

$$g_i^\Omega(\rho) = 2c\sum_{k=0}^L a_k^{(i)}\exp\left\{-\frac{i}{2}z_k^{(i)}\rho^2\right\}, \tag{56}$$

with $\sum_{k=0}^\infty a_k^{(i)} = 1$. L is an arbitrary positive integer and will be let tend to ∞ below. We insert the ansatz (56) into Eq. (45) and use a similar Taylor expansion as above to obtain

$$g_{i+1}^\Omega(\rho) = 2ce^{-2c}\sum_{l_0=0}^\infty \cdots \sum_{l_L=0}^\infty \left(\prod_{k=0}^L \frac{(2ca_k^{(i)})^{l_k}}{l_k!}\right)\exp\left\{-\frac{i}{2}\left(1 + \frac{1}{\Omega - 1 - \sum_{k=0}^\infty l_k z_k^{(i)}}\right)\rho^2\right\}. \tag{57}$$

When we now let $L \to \infty$, we get the expression

$$g_{i+1}^\Omega(\rho) = 2c\sum_{\{(l_k)\}} a_{(l_k)}^{(i+1)}\exp\left(-\frac{i}{2}z_{(l_k)}^{(i+1)}\rho^2\right) \tag{58}$$

with

$$a_{(l_k)}^{(i+1)} = e^{-2c}\prod_{k=0}^\infty \frac{(2ca_k^{(i)})^{l_k}}{l_k!} \tag{59}$$

and

$$z_{(l_k)}^{(i+1)} = 1 + \frac{1}{\Omega - 1 - \sum_{k=0}^\infty l_k z_k^{(i)}} \tag{60}$$

We use the notation (l_k) to denote a whole sequence of non-negative integers, while l_k (without parentheses) denotes the k-th element of the sequence. Out of all possible such sequences we only need those with a *finite* number of non-zero elements. This is because $a_k^{(i)} \to 0$ as $k \to \infty$, and thus $\prod_{k=0}^\infty \frac{(2ca_k^{(i)})^{l_k}}{l_k!} = 0$ if there were infinitely many non-zero elements in (l_k). The set of all sequences with a finite number of non-zero elements is denoted by $\{(l_k)\}$. The summation in Eq. (58) thus goes over a countable set and therefore, $g_{i+1}^\Omega(\rho)$ is of the same functional form as $g_i^\Omega(\rho)$. It is easy to see that $\sum_{\{(l_k)\}} a_{(l_k)}^{(i+1)} = 1$ holds also for the next iteration.

Since $g_2^\Omega(\rho)$ is an expression of the form of Eq. (56), it follows by induction that all $g_i^\Omega(\rho)$, $i \geq 2$, are of the same form. This observation enables us to write down *fix-point* equations for the coefficients a and the exponential prefactors z:

$$a_{(l_k)}^{(i+1)} = a_k^{(i)} \quad \text{and} \quad z_{(l_k)}^{(i+1)} = z_k^{(i)}. \tag{61}$$

As shown in App. B, these equations can be solved if the indices on the left and right hand sides are matched by mapping the sequence (l_k) that appears as index on the left hand side onto a simple number $n = \sum_k l_k M^k$ with some positive integer M. Afterwards, M is taken to infinity. In the process, a new structure of the coefficients a and z emerges: each pair of coefficients (a_i, z_i) falls into one of infinitely many "classes" of increasing complexity. The first three classes are given by the following expressions (the upper index denotes the class), the general form can be found in the appendix:

$$a_0^0 = e^{-2c} \qquad z_0^0 = \frac{\Omega}{\Omega - 1} \tag{62}$$

$$a_n^1 = e^{-2c}\frac{(2ca_0^0)^n}{n!} \qquad z_n^1 = \frac{\Omega - nz_0^0}{\Omega - 1 - nz_0^0} \tag{63}$$

$$a_{(l_k)}^2 = e^{-2c}\prod_{k=0}^{\infty}\frac{(2ca_k^1)^{l_k}}{l_k!} \qquad z_{(l_k)}^2 = \frac{\Omega - \sum_{k=0}^{\infty} l_k z_k^1}{\Omega - 1 - \sum_{k=0}^{\infty} l_k z_k^1}. \tag{64}$$

Note that the expression for a higher class automatically contains all of the lower classes as well if the lower-class expressions are recursively inserted, e.g. $a_{1,0,0,\ldots}^2 = e^{-2c\frac{(2ca_1^1)^1}{1!}} = a_1^1$. This remains true in the general case. For higher classes, the indices become more complicated, e.g. for class 3 it is necessary to use $(l_{(k_i)})$ as index on the left hand sides. As a shorthand, however, it is convenient to use the notation (l_k) or just k even for the higher classes. It is then understood that k itself may stand for a more complicated object like a nested sequence. See App. B for details.

We mention the result that s^m, the sum over all a from classes 0 to m, is given by

$$s^m := \sum_{\{(l_k)\}} a_{(l_k)}^m = e^{-2c}\prod_k e^{2ca_k^{m-1}} = \exp\left\{-2c(1 - s^{m-1})\right\}, \quad \text{and} \tag{65}$$

$$s^0 = e^{-2c} \tag{66}$$

As long as $c < \frac{1}{2}$, the corresponding fixpoint equation, $s = e^{-2c(1-s)}$, has a stable fixpoint at $s = 1$, which implies $\lim_{m\to\infty} s^m = 1$, as it should be. The quantity $1 - s^m$ is therefore a measure for the quality of an approximation that only goes up to class m. We can conclude that for small c only a few classes are sufficient whereas for c close to $\frac{1}{2}$ considerably more are needed. For $c > \frac{1}{2}$, the fixpoint becomes unstable, indicating that the iteration does no longer converge to the full solution of the intergral equation due to the appearance of the infinite cluster.

Implications for the density of states

Making use of the solution just constructed, the resolvent can be written as

$$G(\Omega) = -1 + \lim_{m\to\infty}\sum_k \frac{a_k^m}{z_k^m}. \tag{67}$$

Here, inclusion of a's and z's from classes lower than m in a_k^m and z_k^m has been implied as explained above. Analogous to Eq. (47), this results in the exact density of states

$$D_{\text{tot}}(\gamma) = \lim_{m\to\infty}\sum_k a_k^m \sum_i \frac{\delta(\gamma - \gamma_{ki}^m)}{|\partial z_k^m/\partial\gamma(\gamma_{ki}^m)|}, \tag{68}$$

that is, a sum of δ-peaks located at the roots γ_{ki}^m of the respective $z_k^m(\gamma)$ with weight factors $a_k^m\left|\frac{\partial z_k^m}{\partial\gamma}(\gamma_{ki}^m)\right|^{-1}$. It can be proved with Cauchy's integration theorem applied to $(z_{(l_k)}^m)^{-1}$ and Eq. (64) or the more general expression from App. B that $\sum_i \left|\frac{\partial z_k^m}{\partial\gamma}(\gamma_{ki}^m)\right|^{-1} = 1$ holds for every z_k^m. This property guarantees that the total weight of all peaks in the spectrum is 1 (recall that the sum of all a's is also 1). There is no continuous part of the spectrum, but this would change for $c > \frac{1}{2}$ due to the appearance of an infinite cluster.

It is impossible to find the roots of all z^m but classes 0 and 1 can be solved exactly. We deduce from Eq. (63) that the roots of z_n^1 are located at $\gamma_{n,1} = 0$ and $\gamma_{n,2} = n+1$. The weight factors are easily computed as $\frac{1}{n+1}$ for the peak at 0 and $\frac{n}{n+1}$ for the peak at $n+1$. The density of eigenvalues including class 0 and 1 then reads

$$D^1_{\rm tot}(\gamma) = \frac{e^{2ce^{-2c}}-1}{2c}\delta(\gamma) + \sum_{k=2}^{\infty} \frac{(2ce^{-2c})^k}{2ck(k-2)!}\delta(\gamma - k). \tag{69}$$

Note that this is different from the result of the second iteration, Eq. (55), although it contains the same peaks.

Another consequence of the exact solution of the integral equation is that the density of states does *not* show scaling behavior with respect to c, i.e. it can not be written in the form $D_{\rm tot}(\gamma) \sim f(\gamma/\gamma^*(c))$ with some typical $\gamma^*(c)$. This follows from the fact that the positions of the peaks are given by the roots of the z's which are independent of c and only the weights of the peaks depend on c. This can obviously never result in an exact scaling form: if scaling were valid, a small change of γ^* would result in a small shift of the peak positions, but they must stay fixed. It will be shown below for the fluctuating crosslink strengths that numerical solutions for the eigenvalue density indicate that not even an approximate scaling relation holds. This view will furthermore be supported by the results of the numerical diagonalization of random matrices for different types of systems.

To conclude the discussion of the density of states for uniform crosslink strengths, the spectrum from the iterative solution of the integral equation is compared with results from numerical diagonalization of Γ (for details see Sec. IV below). Fig. 1 shows the numerically computed spectrum for $c = 0.1$. Note that there is a peak at $\gamma = 1$, which is not present in Eq. (69). This "missing peak" can only be found in higher classes, e.g. in $z^2_{0,1,0,\ldots} = \frac{\gamma(\gamma-1)(\gamma-3)}{\gamma^3-5\gamma^2+6\gamma^2-1}$. Other roots that can easily be identified with peaks in the numerical results are at $2 \pm \sqrt{2}$ (stemming from $z^2_{1,1,0,\ldots}$) or at $\frac{5}{2} \pm \frac{\sqrt{5}}{2}$ (stemming from $z^2_{0,2,0,\ldots}$). Fig. 2 shows a direct comparison between the same numerical simulation and a few explicitly calculated peaks from classes up to class 3. The agreement regarding the position of the peaks is excellent but some weight is still missing from some of the peaks. This weight is expected to be found in higher classes and/or in different z's which happen to have a root at the same position.

D. Numerical integration for special $p(\lambda)$

The integral equation (33) simplifies considerably for a special choice of $p(\lambda)$, namely

$$p(\lambda) = \frac{1}{\lambda^2}\exp\left\{-\frac{1}{\lambda}\right\}, \tag{70}$$

implying $P_n = n!$. Inserting the ansatz $g^\Omega(\rho) =: f_\Omega(\rho^2/2)$ into Eq. (34) leads to the following representation

$$G(\Omega) = -1 + \frac{i}{2c}\int_0^\infty {\rm d}x\, f_\Omega(x), \tag{71}$$

where $f_\Omega(x)$ is the solution of the ordinary differential equation (see Appendix A.2 for details)

$$f_\Omega(x) = -i\,x\,f''_\Omega(x) + 2c\,\exp\{-2c + i\Omega\,x + f_\Omega(x)\}\,, \quad f_\Omega(0) = 2c. \tag{72}$$

This allows one to write down the general term in the asymptotic expansion of $G(\Omega)$ for small Ω. Close to the critical point the lowest order moments are explicitly given by

$$M_1 = \frac{1}{4c}\left\{\ln(\frac{1}{1-2c}) - 2c\right\}, \quad c \to \frac{1}{2}, \tag{73}$$

$$M_2 = \frac{2}{15\,(1-2\,c)^3} + \frac{13}{60\,(1-2\,c)^2} + \mathcal{O}((1-2\,c)^{-1}), \quad c \to \frac{1}{2}, \tag{74}$$

$$M_3 = \frac{47}{240\,(1-2\,c)^6} + \frac{16}{105\,(1-2\,c)^5} + \mathcal{O}((1-2\,c)^{-4}), \quad c \to \frac{1}{2}, \tag{75}$$

and

$$M_4 = \frac{5762}{6435\,(1-2\,c)^9} + \frac{1159}{720720\,(1-2\,c)^8} + \mathcal{O}((1-2\,c)^{-7}), \quad c \to \frac{1}{2}, \tag{76}$$

giving additional support to the conjecture about the Lifshitz tail Eq. (40).

For a numerical evaluation of $G(\Omega)$ it is more convenient to rewrite Eq. (33) in the following form,

$$\begin{aligned} g^{\Omega}(\rho) &= 2c\,\sqrt{2i}\,\rho\,\mathrm{K}_1\Big(\sqrt{2i}\,\rho\Big) \\ &+ 4ic\,e^{-2c}\,\rho\,\mathrm{K}_1\Big(\sqrt{2i}\,\rho\Big)\int_0^{\rho} \mathrm{d}\eta\,\mathrm{I}_1\Big(\sqrt{2i}\,\eta\Big)\,\exp\Big\{\frac{i\Omega}{2}\,\eta^2 + g^{\Omega}(\eta)\Big\} \\ &+ 4ic\,e^{-2c}\,\rho\,\mathrm{I}_1\Big(\sqrt{2i}\,\rho\Big)\int_{\rho}^{\infty} \mathrm{d}\eta\,\mathrm{K}_1\Big(\sqrt{2i}\,\eta\Big)\,\exp\Big\{\frac{i\Omega}{2}\,\eta^2 + g^{\Omega}(\eta)\Big\}\,, \end{aligned} \tag{77}$$

since in this representation, the integrands do not depend on ρ and the numerical integration thus needs to be done only once per iteration, resulting in time and memory requirements only of the order of the number of integration grid points. This allows for high precision computations of $g^{\Omega}(\rho)$, $G(\Omega)$, and $D(\gamma)$.

Figures 3 and 4 show the results for the density of eigenvalues from a numerical integration of Eq. (77) using a Padé approximation in order to extrapolate $\Omega = \gamma + i\epsilon$ to $\epsilon = 0$. There are several noteworthy points to be seen in these figures:

First, we expect to see Lifshitz tails for *all* c, $0 < c < 1/2$, for asymptotically small γ. Precisely at the critical point $D(\gamma)$ goes to a constant as $\gamma \to 0$. For crosslink concentrations close to the critical one, we expect to see a crossover between an approximately constant region at intermediate γ to a Lifshitz tail at very small γ. Since small values of γ are hard to access numerically, this crossover makes it difficult to observe the Lifshitz tail, except possibly for small c. For intermediate c the data in Fig. 4 can be described approximately by a straight line but with a slope different from $-\frac{1}{2}$. This property will be confirmed by the results from the numerical diagonalization presented below.

A second remarkable point is that the density of states as seen in Fig. 3 is clearly not suited to a scaling ansatz. There are (at least) two different scales contained in the plot: the first is the drop-off length $\gamma^0(c)$ which describes the scale on which $D(\gamma)$ goes to 0 for small γ, the other is the position of the maximum, $\gamma^{\max}(c)$. While γ^0 goes to 0 for $c \to \frac{1}{2}$, $\gamma^{\max}$ evidently does not; these two features together are obviously incompatible with a scaling ansatz of the form $D(\gamma) \sim f(\gamma/\gamma^*(c))$ with some typical γ^*. This finding is in agreement with the observation from the exact solution for uniform crosslink strength where scaling was not possible either. Here, however, the statement is even stronger than in the previous case since even an approximate scaling relation is ruled out. Note the peculiar feature that a second maximum appears in $D(\gamma)$ for small γ at the percolation threshold $c = \frac{1}{2}$. This is not an artifact and is confirmed by the numerical diagonalization as shown below. It may even indicate the presence of a third scale since the emergence of a maximum can already be suspected in the curves for smaller c.

E. Stress relaxation

The characteristic features of the spectrum as discussed above, have important consequences for the stress relaxation function. In particular the Lifshitz tail in the spectrum gives rise to an anomalous long time decay of the stress relaxation function in the sol phase for all $c < c_{crit}$. The true asymptotic behaviour of $D(\gamma) \sim \exp(-\sqrt{h(c)/\gamma})$, which is proven rigorously in Appendix A.3, implies $\chi(t) \sim \exp(-(t/\tau^*)^{\beta})$ with $\beta = 1/3$. However we are unable to estimate the timescale needed to reach the asymptotic regime. For smaller times, the stress relaxation function is characterized by effective exponents, just like the spectra in Figs. 4,7 can be fitted to Lifshitz tails with effective exponents that depend on crosslink concentration c.

The divergence of the timescale $\tau^*(\epsilon) \sim \epsilon^{-z}$ is determined by the function $h(c)$. The expansion of the resolvent for small Ω suggests $z = 3$. At the critical point the density of eigenvalues is constant as $\gamma \to 0$, implying a logarithmic divergence of the static shear viscosity and $\chi(t) \sim t^{-\Delta}$ with $\Delta = 1$.

The absence of scaling in the density of states is also relevant for the stress relaxation function. The presence of more than one characteristic scale for the eigenvalues implies more than one characteristic timescale for the stress relaxation function. As a consequence, the stress relaxation function does not scale either. This point will be discussed further below in the context of numerical diagonalization of the connectivity matrix. Attempts to scale data for the time dependent stress relaxation function fail, see Fig. 15.

IV. NUMERICAL DIAGONALIZATION

A. Numerical methods

In this section the eigenvalue densities $D(\gamma)$ of three different types of random networks are studied numerically: mean-field (MF) networks as well as two- and three-dimensional simple square/cubic grids. For the first case, crosslinks are allowed for all pairs i, j of nodes while for the other networks only crosslinks between neighboring nodes may appear. For the finite-dimensional grids we apply periodic boundary conditions in all directions. The size of the networks is denoted by N, with $N = L^d$ $(d = 2, 3)$ for the finite-dimensional cases. For the numerical treatment, we consider random graphs with a fixed number M of vertices, i.e. the crosslink concentration is $c = M/N$. Every crosslink has the same probability of occurrence. For the implementation of the graphs on the computer, the LEDA library[17] was used. Network sizes up to $N = 10000$ (MF), $N = 3136$ $(d = 2)$ and $N = 4096$ $(d = 3)$ where studied. For each system size up to 10^4 different realizations of the disorder were considered (1000 for the largest sizes). Different concentrations of the crosslinks between 0 and the percolation threshold c_{crit} were treated, where $c_{\text{crit}}(\text{MF}) = 1/2$, $c_{\text{crit}}(d = 2) = 1$ and $c_{\text{crit}}(d = 3) \approx 0.7464$[18].

We consider the same two cases regarding the strength of the crosslinks as above: Either all crosslinks have the same strength $\lambda = 1$ or their strengths are distributed randomly with the probability density given in (70). Numerically, the random values for the strengths of the crosslinks are drawn using the inversion method[19]. A random number r is drawn which is uniformly distributed in $[0, 1]$. Then the values of $\lambda := -1/\ln r$ are distributed according to (70). For testing purposes also some systems were studied where the strengths were uniformly distributed in the interval $[0.5, 1.5]$. In all cases no significant deviations of the measurable quantities for different distributions could be observed. The main difference is that for crosslinks of unit strength the distribution $D(\gamma)$ of the eigenvalues is dominated by a sum of delta-peaks below the percolation threshold while for crosslinks of continuous strength the distribution $D(\gamma)$ is purely continuous (see below).

The numerical method works as follows: Random networks are created, with constant or random crosslink strengths as needed. Then, for each graph the connected components are determined[20]. For each connected component the connectivity matrix is calculated, which is a real symmetric matrix. Therefore, for determining its eigenvalues the QR algorithm and the Householder method[21] can be applied. Next, the eigenvalues are sorted in increasing order. Each connected component has one smallest eigenvalue 0. Because of numerical errors usually the smallest eigenvalue is not zero but quite small, depending on the distribution of the strengths of the crosslinks. Consequently, the smallest eigenvalue is assigned the value zero. Finally, the eigenvalues of all components are collected, sorted again, and stored for further evaluation for each realization of the network.

B. Results for the mean-field system

First, we consider the density $D(\gamma)$ of non-zero eigenvalues for the mean-field network at the percolation threshold $c = 1/2$. Data for the case $p(\lambda) = \delta(\lambda - 1)$ have already been presented in Fig. 1. Here we consider the case where the strengths of the crosslinks are distributed according Eq. (70). In Fig. 5 the resulting density is shown for different system sizes together with the analytical result (obtained from the numerical solution of Eq. (77)). It can be seen that the size $N = 10000$ is already sufficient to find the analytical behavior for a large range of eigenvalues. Especially the "dip" near $\gamma = 0.15$ is validated by the numerical data (see inset). Because of the finite system sizes, arbitrarily small eigenvalues cannot be found, thus the numerics disagree from the analytical result in that region. Later we will see that this raises several problems when studying dynamical properties of the networks. Nevertheless, the analytical result $\lim_{\gamma\to 0} D(\gamma) > 0$ can indeed be confirmed by extrapolating the numerical data to the infinite system size.

The behavior of $D(\gamma)$ for different crosslink concentrations c is presented in Fig. 6. Once more, the numerical $(N = 10000)$ and the analytical results agree very well. For small γ, the logarithm of the density should behave as $\sim -\gamma^{-1/2}$ (Lifshitz tail). Fig. 7 shows the logarithm of $D(\gamma)$ in a double logarithmic plot in complete analogy to the solution of the integral equation (Fig. 4). Presumably, the system size of $N = 10000$ is still too small in order to observe the asymptotic behavior of the density of states for small eigenvalues.

C. Results for the finite-dimensional systems

Now we consider three-dimensional systems, which are believed to describe real polymer networks more appropriately. The density of eigenvalues for the case where all crosslinks have the same strength, $p(\lambda) = \delta(\lambda - 1)$, is shown in Fig. 8 for $N = 16^3$ and $c = 0.2$. Similar to the mean-field case, a collection of delta-peaks is obtained. Since this kind of distribution is more difficult to analyze, we turn again to the model where the strengths of the bonds have the broad distribution (70). Results for the largest system size $N = 16^3$ and different crosslink concentrations are shown in Fig. 9. Below the percolation transition $c_{\rm crit} \approx 0.7464$ the distribution exhibits a maximum and converges to 0 for small eigenvalues, similar to the mean-field case. But at the transition $D(\gamma)$ diverges when the zero eigenvalue is approached (see also inset). Below we will show that this behavior changes the divergence of the viscosity near the percolation threshold. The eigenvalue densities for the two-dimensional network look qualitatively similar and are therefore not shown here. The true asymptotic behavior as $\gamma \to 0$ is difficult to access, just as in the mean-field case.

The changes in the spectrum as compared to the mean-field case also effect the stress relaxation, that we investigate next. First, the viscosity given by

$$\overline{\eta} = (1 - T_0(c)) \int_0^\infty \frac{D(\gamma)}{\gamma}\, d\gamma \tag{78}$$

is considered. Here, irrelevant prefactors have been omitted for simplicity, cf. Eq. (18) for the complete expression. In the numerical calculation we compute

$$\eta = \frac{1}{N} \sum_{\gamma_i > 0} \frac{1}{\gamma_i} \tag{79}$$

for each realization and subsequently average over different realizations of the disorder to obtain $\overline{\eta}$. Whereas for the mean-field network the viscosity diverges logarithmically for $c \to c_{\rm crit}$, for finite-dimensional systems a divergence $\eta(c) \sim (c_{\rm crit} - c)^{-k}$ is expected. The reason for the different divergencies is the manner in which $D(\gamma)$ behaves for small γ at the percolation threshold: for the mean-field network, $\lim_{\gamma\to 0} D(\gamma)$ is finite, but for the finite-dimensional grids $D(\gamma)$ diverges as $\gamma \to 0$. The exponent k, which describes the viscosity near the percolation threshold, can be determined, similar to the usual finite-size scaling relations[22] for the percolation transition, from

$$\eta(c, L) = L^{-k/\nu} \tilde{\eta}((c - c_{\rm crit}) L^{1/\nu}) \,, \tag{80}$$

where $\tilde{\eta}$ is a universal function and ν is the exponent describing the divergence of the correlation length when approaching the percolation transition. The use of finite-size scaling enables us to circumvent the problems which are posed by the lack of very small eigenvalues of finite graphs.

By plotting $\eta L^{k/\nu}$ against $(c - c_{\rm crit})L^{1/\nu}$ with correct parameters ν and k the datapoints for different system sizes for $c \approx c_{\rm crit}$ should collapse onto a single curve. We have taken the values $\nu(d = 2) = 4/3$ and $\nu(d = 3) = 0.88$ from the literature[18] and adjusted k/ν. The best collapse near $c_{\rm crit}$ was obtained with $k(d = 2) = 1.19$ and $k(d = 3) = 0.75$. The results are presented in Figs. 10 ($d = 3$) and 11 ($d = 2$). The values we have obtained for the different distributions of the crosslink strengths agree within the error bars.

The value of k for two dimensions agrees very well with the result $k \sim 1.17$ found previously by Broderix et al.[10], using the high precison simulations of Gingold et al.[12]. The result for the three-dimensional case ($k = 0.75$)is slightly worse in comparison with $k \sim 0.71$[10,12]. The reason is that here only small system sizes up to 20^3 could be treated due to the fact that all eigenvalues are calculated. If one is only interested in k, it is computationally less expensive to compute the Moore-Penrose inverse of the connectivity matrix. Thereby one might be able to study system sizes as large as those used in Ref.[12]. For the realizations treated here, we have checked other characteristic results concerning the percolation transition, like the critical exponent σ, which describes the behavior of the cluster-size distribution. The finite-size scaling plots have a poor quality for this quantity, too, resulting in a rather low precision of the exponent values. Additionally, we have observed a systematic drift in our results: By including even smaller system sizes, the scaling plot results in $k = 0.89$ which differs even more from the value obtained before. Consequently, we believe that larger system sizes are needed, to obtain a more reliable result for k via numerical diagonalization of random connectivity matrices.

Next, the behavior of the stress relaxation function (again omitting irrelevant prefactors and using dimensionless time $\frac{2dt}{\zeta a^2} \to t$)

$$\chi(t) = (1 - T_0(c)) \int_0^\infty D(\gamma) \exp(-\gamma t)\, d\gamma \tag{81}$$

is investigated, see Eq. (17) for the complete expression. The functions were obtained by first calculating $D(\gamma)$ and then numerically integrating it. It would take too much time on the computer to first calculate $\chi(t)$ for each realization by directly summing up the contributions and then average over the disorder. Here, we have investigated the systems with the continuously distributed crosslink strengths because they result in continuous eigenvalue densities where it is easier to obtain stable numerical data.

In Fig. 12 the numerical results for the mean-field network, the $d = 2$ and the $d = 3$ model for the largest sizes ($c = c_{\rm crit}$) are shown. As mentioned before, the numerical simulations are restricted to finite sizes of the networks and to a finite number of realizations of the disorder. Therefore, the eigenvalue densities $D(\gamma)$ always have a smallest eigenvalue $\gamma_{\rm min}$ with $D(\gamma) = 0$ for $\gamma < \gamma_{\rm min}$. Consequently, the long-time behavior is dominated by an exponential decrease, $\exp(-\gamma_{\rm min} t)$, irrespective of the true form of $\chi(t)$. This results in a negative curvature in the double-logarithmic plot for long times. Thus, in the numerical results, the asymptotic form of the relaxation function is visible only for intermediate times (see Fig. 12). At $c = c_{\rm crit}$ a $\chi(t) \sim t^{-\Delta}$ behavior is expected. By fitting we obtain $\Delta = 1.029(5)$ (mean field), $\Delta = 0.830(2)$ ($d = 3$), and $\Delta = 0.741(2)$ ($d = 2$). The results for the mean-field case is known exactly to be $\Delta = 1$. The discrepancy comes again from the finite sizes of the networks: Indeed, we have observed that for smaller networks a value of the exponent is obtained which is even larger. So the result $\Delta = 1$ seems to be confirmed. The value for the three-dimensional grid is compatible with the large range of results obtained in experiments[5].

The behavior of $\chi(t)$ for different concentrations c of the crosslinks is shown in Figs. 13 (mean-field) and 14 ($d = 3$). In both cases we find exponential decay for the longest times due to finite system size. For intermediate times a stretched exponential behavior $\chi(t) \sim \exp(-(t/\tau)^{\beta})$ is visible. At least for finite system sizes the exponent β seems to be non-universal, we find values ranging from $\beta = 0.5$ for small crosslink concentrations down to $\beta = 0.2$ close to the percolation threshold. We suspect that the accessible times are too short to see the true asymptotic behaviour, which at least in mean-filed theory is known to be a stretched exponential with exponent $\beta = 1/3$, resulting from the Lifshitz tail in the density of states. For small times $\chi(t)$ decreases like $t^{-\Delta}$ and $\chi(0) = 1$ by definition.

Moreover, this variation of the exponent β makes it impossible to observe a scaling form $\chi(t) \sim t^{-\Delta} g(t/\tau)$, were τ is a typical time scale which diverges like $\tau \sim (c_{\rm crit} - c)^{-z}$ when approaching the percolation threshold. For the mean-field network, the expectations from the Lifshitz tails are $z = 3$ and $\Delta = 1$, while $g(t)$ is the stretched exponential function, but it was already mentioned that there seems to be no scaling possible due to the existence of more than one scale. In Fig. 15 a scaling plot of $\chi(t)$ is shown. $\chi(t)t^{\Delta}$ is plotted against $t \times (c_{\rm crit} - c)^{z}$ for mean-field networks having different concentrations c. We have used only the regions below the finite-size asymptotic behavior ($\beta = 1$). It can be seen that the quality of the collapse is rather bad, explained by the variation of β with c. One might think that near the transition $c \approx c_{\rm crit}$ the scaling may be better. But there the collapse is even worse (not shown), because even larger systems are necessary to reach the asymptotic regime for the small eigenvalues, as explained before.

For the finite-dimensional systems, the quality of the scaling-plot is similar. Therefore, it is not possible to make a reliable estimate for the dynamical exponent z in that case.

V. CONCLUSIONS

Within our model, the dynamics of a crosslinked polymer melt is determined completely by the eigenvalue and eigenvector spectrum of the connectivity matrix Γ. In this paper we have focused on some properties which are determined by the eigenvalues alone (e.g. the stress relaxation function) since the eigenvectors are hard to obtain. We have used three different methods to examine the eigenvalue spectrum: First, the construction of an exact solution for the averaged eigenvalue density for a fixed crosslink strength, second, a very precise numerical solution for the case of varying crosslink strengths, and third, a numerical diagonalization of random connectivity matrices.

The first method allowed for some exact results regarding the eigenvalue spectrum. It could be shown that the eigenvalue spectrum consists of a very complicated but countable set of δ-peaks, some of which could be calculated and compared with results from numerical diagonalization. Furthermore it showed that the eigenvalue density does not show (exact) scaling behavior.

The second model of fluctuating crosslink strengths has the advantage that the eigenvalue spectrum becomes a continuous function instead of an inscrutable sum of δ-peaks. Additionally, it allowed for a fast numerical integration scheme. From these numerical solutions it could be inferred that the expected Lifshitz-tail behavior for small γ only seems to set in for extremely small γ, smaller than were accessible numerically. For this reason, the stress relaxation function does not show a stretched exponential form with exponent $\beta = \frac{1}{3}$ within the accessible time window. Instead, for the times that could be reached, there seems to be a regime where an apparent stretched exponential with a crosslink concentration-dependent and thus non-universal β can be observed. Furthermore, in numerical evaluations of the eigenvalue spectrum again scaling could not be observed, not even approximately, since at least two, possibly three or more, different γ-scales with different c-dependence could be identified. As a consequence, the stress relaxation function does not scale either.

The third method, numerical diagonalization, confirmed all results obtained so far very well. In particular it showed that the stress relaxation shows stretched-exponential behavior with a concentration-dependent exponent β and it showed the failure of scaling of the stress relaxation function. It confirmed, however, the experimental findings that at the critical concentration, the stress relaxation function decays algebraically with exponent Δ. For the mean-field model, both theory and numerics yield the exponent $\Delta = 1$. Furthermore, numerical diagonalization allows for going beyond the mean-field approach. Results were obtained for connectivity matrices on two- and three-dimensional cubic lattices. Unlike the mean-field case, the density of eigenvalues now diverges at the critical concentration as $\gamma \to 0$. Apart from this difference, the other results are qualitatively very similar to the mean-field case except that the exponents Δ and β have different values.

VI. ACKNOWLEDGEMENTS

We thank P. Müller for interesting discussions and a careful reading of the manuscript. K.B. obtained financial support by the DFG (*Deutsche Forschungsgemeinschaft*) under grant Br 1894/1-1 , T.A. under grant Zi209/5-1 and A.K.H. under grant Zi209/6-1.

APPENDIX A: LOW FREQUENCY EXPANSION OF THE RESOLVENT

1. General $p(\lambda)$

The low frequency expansion is derived from an alternative form of the integral equation (33). We start from Eq. (30) and recall an integral representation of the n-dimensional Laplacian (see also Eqs. (3.47-51)) in Ref. 13

$$\int \frac{d\hat{y}}{(2\pi\Omega)^{n/2}} \exp\left\{-\frac{(\hat{x}-\hat{y})^2}{2\Omega}\right\} f(|\hat{y}|) = \exp\left\{\frac{\Omega}{2}\left(\frac{d^2}{d\rho^2} + \frac{n-1}{\rho}\frac{d}{d\rho}\right)\right\} f(\rho)\Big|_{\rho=|\hat{x}|} . \tag{A1}$$

We use this representation in the numerator of Eq. (30) and take the limit $n \to 0$. To evaluate the denominator of Eq. (30) we observe that

$$\lim_{n\to 0} \int d\hat{x} f_n(|\hat{x}|) = f_0(0) + \mathcal{O}(n). \tag{A2}$$

Both steps taken together lead to the following self-consistent equation for $g^{\Omega}(\rho)$

$$g^{\Omega}(\rho) = 2c\, e^{-2c} \int_0^{\infty} \mathrm{d}\lambda\, p(\lambda) \exp\left\{\frac{1}{2i\lambda}\left(\frac{\partial^2}{\partial\rho^2} - \frac{\partial}{\rho\,\partial\rho}\right)\right\} \exp\left\{\frac{i\Omega}{2}\rho^2 + g^{\Omega}(\rho)\right\}, \tag{A3}$$

which is of course equivalent to the integral equation (33), but much better suited for a low frequency expansion.

To that end we rescale variables according to $x = \sqrt{\Omega}\rho$ and $\Psi^{\Omega}(x) = g^{\Omega}(x/\sqrt{\Omega})$. The self consistent equation then reads

$$\Psi^{\Omega}(x) = 2c\, e^{-2c} \int_0^{\infty} \mathrm{d}\lambda\, p(\lambda) \exp\left\{\frac{\Omega}{2i\lambda}\left(\frac{\partial^2}{\partial x^2} - \frac{\partial}{x\,\partial x}\right)\right\} \exp\left\{\frac{i}{2}x^2 + \Psi^{\Omega}(x)\right\}. \tag{A4}$$

We look for a solution in terms of a power series in Ω

$$\Psi^{\Omega}(x) = \sum_{j=0}^{\infty} (\Omega)^j \Psi_j(x). \tag{A5}$$

The resolvent can then be expressed in terms of $\Psi_j(x)$ as follows

$$G(\Omega) = -P_1 + \frac{i}{2c\Omega} \sum_{j=0}^{\infty} \Omega^j \int_0^{\infty} dx x \Psi_j(x) \tag{A6}$$

with $P_n = \int_0^{\infty} \mathrm{d}\lambda \lambda^{-n} p(\lambda)$ as defined after Eq. (38). The lowest order term obeys the equation

$$\Psi_0(x) = 2c \exp(-2c) \exp\left(\frac{i}{2}x^2 + \Psi_0(x)\right), \tag{A7}$$

which is solved by

$$\Psi_0(x) = -W\left(-2c\exp\left(-2c\right)\exp\left(ix^2/2\right)\right). \tag{A8}$$

Here W denotes the principal branch of Lambert's W-function, defined as the solution of

$$W(x)\exp\left(W(x)\right) = x. \tag{A9}$$

From Eq. (A7) one derives the following property of the lowest order solution

$$\Psi_0'(x) = \frac{ix\Psi_0(x)}{1-\Psi_0(x)} \tag{A10}$$

which allows for an exact computation of the integral

$$i\int_0^\infty dx x\Psi_0(x) = -\frac{1}{2}\int_0^\infty dx\frac{d}{dx}\left(1-\Psi_0(x)\right)^2 = 2c(c-1). \tag{A11}$$

The next two terms are given by

$$\Psi_1(x) = \frac{1}{1-\Psi_0(x)}\frac{P_1}{2i}\left(\frac{d^2}{dx^2}-\frac{d}{x\,dx}\right)\Psi_0(x) \tag{A12}$$

$$\Psi_2(x) = \frac{-1}{1-\Psi_0(x)}\left(\frac{d^2}{dx^2}-\frac{d}{x\,dx}\right)\left(\frac{P_2}{8}+\frac{P_1^2}{1-\Psi_0(x)}\right)\left(\frac{d^2}{dx^2}-\frac{d}{x\,dx}\right)\Psi_0(x). \tag{A13}$$

The integrals $\int dx x\Psi_j(x)$ can be performed similar to Eq. (A11), using the properties of Lambert's W-function. The computations, however, become increasingly tedious, so that higher order terms have only been computed for the special distribution $p(\lambda)$, see below.

2. Special $p(\lambda)$

We start from Eq. (A3) and introduce the abbreviation $D_\rho := \frac{d^2}{d\rho^2} - \frac{d}{\rho\,d\rho}$. For the special choice $p(\lambda) = \frac{1}{\lambda^2}\exp\left(-1/\lambda\right)$, one can perform the average over $p(\lambda)$ analytically

$$\int_0^\infty \frac{d\lambda}{\lambda^2}\exp\left\{-\frac{(1+iD_\rho/2)}{\lambda}\right\}\exp\left\{\frac{i\Omega}{2}\rho^2 + g^\Omega(\rho)\right\} = \left(1+\frac{iD_\rho}{2}\right)^{-1}\exp\left\{\frac{i\Omega}{2}\rho^2+g^\Omega(\rho)\right\}. \tag{A14}$$

The resulting differential equation simplifies, if we introduce the function $f_\Omega(\rho^2/2) := g^\Omega(\rho)$

$$f_\Omega(\rho^2/2) + i\rho^2/2 f_\Omega''(\rho^2/2) = 2c\exp\left(-2c\right)\exp\left(i\Omega\rho^2/2 + f_\Omega(\rho^2/2)\right). \tag{A15}$$

Introducing the new variable $x=\rho^2/2$ leads to the differential Eq. (72) quoted in the main part of the paper. For the low frequency expansion it is convenient to introduce yet another variable, $y=\Omega x$, in terms of which the differential equation for $h_\Omega(\Omega x) := f_\Omega(x)$reads

$$h_\Omega(y) - iy\Omega h_\Omega''(y) = 2c\exp\left(-2c\right)\exp\left(iy+h_\Omega(y)\right). \tag{A16}$$

The ansatz $h_\Omega(y) = \sum_{j=0}^\infty (\Omega)^j h_j(y)$ then yields

$$h_n(y) - iyh_{n-1}''(y) = h_0(y)\frac{1}{n!}\frac{d^n}{d\Omega^n}\exp\left.\left(\sum_{j=1}^\infty (\Omega)^j h_j(y)\right)\right|_{\Omega=0}. \tag{A17}$$

The left hand side is linear in $h_n(y)$, so that Eq. (A17) is easily iterated.

3. Proof of the existence of a Lifshitz tail in $D(\gamma)$

The aim of this appendix is to prove that the density of eigenvalues $D(\gamma)$ shows a Lifshitz-tail behavior for $\gamma \to 0$ and $c < 1/2$. For the proof, it is convenient to make use of the eigenvalue distribution function, $F(\gamma) := \int_{-\infty}^{\gamma} \mathrm{d}\gamma' \, D(\gamma')$. This can be done without loss of generality because if $F(\gamma)$ has a Lifshitz tail, so does $D(\gamma)$. It will be shown that $F(\gamma)$ lies between two bounds which, taken together, assert the Lifshitz behavior.

For a given realization of a system with N vertices (or polymers), the corresponding $F_N(\gamma)$ can be written, using a decomposition into the K clusters of the realization,

$$F_N(\gamma) = \frac{1}{N} \sum_{k=1}^{K} \operatorname{Tr} \Theta(\gamma - \Gamma_k) = \frac{K}{N} + \frac{1}{N} \sum_{k=1}^{K} \operatorname{Tr}[(1 - E_0^k)\Theta(\gamma - \Gamma_k)] \tag{A18}$$

where Γ_k is the connectivity matrix of the k-th cluster and E_0^k is the projector on the nullspace of Γ_k. In the macroscopic limit, $N \to \infty$, this yields

$$F(\gamma) = (1-c)\Theta(\gamma) + \sum_{n=1}^{\infty} \tau_n \left\langle \operatorname{Tr}[(1 - E_0^n)\Theta(\gamma - \Gamma(\mathcal{T}_n))] \right\rangle \tag{A19}$$

due to self-averaging. The bracket $\langle \cdots \rangle$ means averaging over the set of all numbered trees $\{\mathcal{T}_n\}$ of size n of which there are n^{n-2}. $\Gamma(\mathcal{T}_n)$ denotes the connectivity matrix corresponding to the tree $\mathcal{T}_n$. The average number of trees of size n per vertex is denoted by τ_n and is given by[15]

$$\tau_n = \frac{n^{n-2}}{2cn!}(2ce^{-2c})^n = \frac{1}{2c\sqrt{2\pi}} n^{-5/2} e^{-nh(c) - f(n)/n} \tag{A20}$$

according to Stirling's formula with $h(c) = 2c - 1 - \ln(2c)$ and some function $f(n)$ with $0 < f(n) < 1$.

The smallest non-zero eigenvalue of $\Gamma(\mathcal{T}_n)$ is certainly greater than or equal to the smallest non-zero eigenvalue of the linear cluster with n vertices, which is proportional to n^{-2}, i.e.

$$\Gamma(\mathcal{T}_n) \geq \frac{\alpha}{n^2} \tag{A21}$$

(except for the zero eigenvalue) with some α independent of n. This results in

$$\operatorname{Tr}[(1 - E_0^n)\Theta(\gamma - \Gamma(\mathcal{T}_n))] \leq (n-1)\Theta(\gamma - \alpha/n^2) \tag{A22}$$

or

$$F(\gamma) \leq 1 - c + \sum_{n \geq \sqrt{\alpha/\gamma}} (n-1)\tau_n, \quad \text{for } \gamma > 0. \tag{A23}$$

For $\gamma \to 0$, the sum can be approximated by an integral,

$$F(\gamma) \leq 1 - c + \frac{1}{2c\sqrt{2\pi}} \int_{\sqrt{\alpha/\gamma}}^{\infty} n^{-3/2} e^{-nh(c)} \tag{A24}$$

$$\approx 1 - c + \frac{1}{2ch(c)\sqrt{2\pi}} \left(\frac{\gamma}{\alpha}\right)^{3/4} \exp\left\{ -h(c) \left(\frac{\alpha}{\gamma}\right)^{1/2} \right\}. \tag{A25}$$

This is the lower bound for $F(\gamma)$.

For the upper bound, Eq. (A19) will be used again. Explicitly, one has for $\gamma > 0$

$$F(\gamma) = 1 - c + \frac{1}{2c} \sum_{n=1}^{\infty} \frac{1}{n!}(2ce^{-2c})^n \sum_{\{\mathcal{T}_n\}} \operatorname{Tr}[(1 - E_0^n)\Theta(\gamma - \Gamma(\mathcal{T}_n))] \tag{A26}$$

$$\geq 1 - c + \frac{1}{2c} \sum_{n=1}^{\infty} \frac{1}{n!}(2ce^{-2c})^n \sum_{\{\mathcal{L}_\backslash\}} \operatorname{Tr}[(1 - E_0^n)\Theta(\gamma - \Gamma(\mathcal{L}_\backslash))] \tag{A27}$$

where the inner sum has been restricted on the set of *linear* numbered trees $\{\mathcal{L}_\backslash\}$. There are $n!/2$ such linear trees, such that

$$F(\gamma) = 1 - c + \frac{1}{4c} \sum_{n=2}^{\infty} e^{-n(h(c)+1)} \operatorname{Tr}[(1 - E_0^n)\Theta(\gamma - \Gamma(\mathcal{L}_\backslash))]. \tag{A28}$$

Next, the trace, which is a sum of non-negative terms, is estimated by just one of the terms. In particular, $\operatorname{Tr}[(1 - E_0^n)\Theta(\gamma - \Gamma(\mathcal{L}_\backslash))] \geq \Theta(\gamma - \alpha/\backslash^{\in})$, corresponding to the smallest eigenvalue of $\mathcal{L}_\backslash$. This finally gives

$$F(\gamma) \geq 1 - c + \frac{1}{4c} \sum_{n \geq \sqrt{\alpha/\gamma}} e^{-n(h(c)+1)} \tag{A29}$$

$$\approx 1 - c + \frac{1}{2c(1+h(c))} \exp\left\{ -\left(\frac{\alpha}{\gamma}\right)^{1/2} (1 + h(c)) \right\} \tag{A30}$$

for the lower bound.

The upper and the lower bound together imply

$$\lim_{\gamma \to 0} \frac{\ln|\ln(F(\gamma) - 1 + c)|}{|\ln \gamma|} = \frac{1}{2} \tag{A31}$$

or, even stronger,

$$\sqrt{\alpha} h(c) \leq -\lim_{\gamma \to 0} \gamma^{1/2} \ln(F(\gamma) - 1 + c) \leq \sqrt{\alpha}(h(c) + 1), \tag{A32}$$

which is the sought-for Lifshitz tail behavior.

APPENDIX B: DETAILS OF THE EXACT SOLUTION OF THE INTEGRAL EQUATION

1. Solution of the integral equation

It is not obvious how to solve the fix-point equations (61), because the coefficients of the i-th iteration are labeled by an index, and a subsequent iteration gives rise to coefficients which are labelled by a sequence (l_k). We therefore try to map the sequence (l_k) that appears as index onto a number by writing $n := \sum_{k=0}^{\infty} l_k M^k$ with some $M \in \mathbb{N}$. For this to be a one-to-one map, we need to restrict all l_k to be $< M$. This restriction will be removed later when we let $M \to \infty$. The sequence (l_k) can be reconstructed from n by writing n in the number system of base M. Let this be indicated by $l_k = (n)_k^M$.

The fix-point equations can now be written down as:

$$a_n = e^{-2c} \prod_{k=0}^{\infty} \frac{(2ca_k)^{(n)_k^M}}{(n)_k^M!} \tag{B1}$$

$$z_n = 1 + \frac{1}{\Omega - 1 - \sum_{k=0}^{\infty} (n)_k^M z_k}. \tag{B2}$$

The equations for a_n can be solved independently from those for z_n. We start with a_n. Successively solving the system of equations (B1) by inspection gives

$$a_0 = e^{-2c} \tag{B3}$$

$$a_n = e^{-2c} \frac{(2ca_0)^n}{n!} \quad \text{for } 1 \leq n < M \tag{B4}$$

$$a_n = e^{-2c} \prod_{k=0}^{M-1} \frac{(2ca_k)^{(n)_k^M}}{(n)_k^M!} \quad \text{for } M \leq n < M^M \tag{B5}$$

$$a_n = e^{-2c} \prod_{k_0=0}^{M-1} \cdots \prod_{k_{M-1}=0}^{M-1} \frac{(2ca_{k_0 + Mk_1 + \cdots + M^{M-1}k_{M-1}})^{(n)_{k_0+Mk_1\cdots}^M}}{(n)_{k_0+Mk_1\cdots}^M!} \quad \text{for } M^M \leq n < M^{M^M} \tag{B6}$$

and so on. The coefficient a_0 is obviously independent of all other a_n. This property will be called "class 0". $a_1, \dots, a_{M-1}$ only depend on a_0: this will be termed "class 1". Analogously, $a_M, \dots, a_{M^M-1}$ are in class 2 as they only depend on a's from classes 0 and 1.

Now we can let M tend to infinity. Classes 0 and 1 are simple (the upper index now denotes the class):

$$a_0^0 = e^{-2c} \tag{B7}$$

$$a_n^1 = e^{-2c}\frac{(2ce^{-2c})^n}{n!}, \quad n \geq 1 \tag{B8}$$

If we drop the constraint $n \geq 1$, Eq. (B8) automatically contains class 0.

For the higher classes, as we are now considering $M \to \infty$, indexing via a number n is no longer possible. Instead, for class 2, we have to revert to using a finite sequence as index. For class 3, even this is not sufficient and a nested sequence $(l_{(k_i)})$ is needed:

$$a^2_{(l_k)} = e^{-2c}\prod_{k=0}^{\infty}\frac{(2ca_k^1)^{l_k}}{l_k!}, \quad \text{length of } (l_k) > 1, \tag{B9}$$

$$a^3_{(l_{(k_i)})} = e^{-2c}\prod_{\{(k_i)\}}\frac{(2ca^2_{(k_i)})^{l_{(k_i)}}}{l_{(k_i)}!}. \tag{B10}$$

If the constraint (length of $(l_k) > 1$) is dropped and if the explicit expressions for the a from the lower classes are recursively inserted, all classes up to class 2 are contained in one formula, Eq. (B9). An analogous statement holds for Eq. (B10).

In general, for class m, the index will be of the form $(l_{(k_{\ddots_{(r_i)}})})$ with m nesting levels. The general result is thus

$$a^m_{(l_{(k_{\ddots_{(r_i)}})})} = e^{-2c}\prod_{\{(k_{\ddots_{(r_i)}})\}}\frac{\left(2ca^{m-1}_{(k_{\ddots_{(r_i)}})}\right)^{l_{(k_{\ddots_{(r_i)}})}}}{l_{(k_{\ddots_{(r_i)}})}!}. \tag{B11}$$

With the same reasoning as above we can calculate the z_n. We find the same classes, and the results are:

$$z_0^0 = \frac{\Omega}{\Omega - 1} \tag{B12}$$

$$z_n^1 = \frac{\Omega - nz_0^0}{\Omega - 1 - nz_0^0} \tag{B13}$$

$$z^2_{(l_k)} = \frac{\Omega - \sum_{k=0}^{\infty} l_k z_k^1}{\Omega - 1 - \sum_{k=0}^{\infty} l_k z_k^1} \tag{B14}$$

$$\vdots$$

$$z^m_{(l_{(k_{\ddots_{(r_i)}})})} = \frac{\Omega - \sum_{\{(k_{\ddots_{(r_i)}})\}} l_{(k_{\ddots_{(r_i)}})} z^{m-1}_{(k_{\ddots_{(r_i)}})}}{\Omega - 1 - \sum_{\{(k_{\ddots_{(r_i)}})\}} l_{(k_{\ddots_{(r_i)}})} z^{m-1}_{(k_{\ddots_{(r_i)}})}}. \tag{B15}$$

2. Properties of the solution

If one asks for the total weight of a particular peak at, say, some γ_0 (up to class m), one has to find all finite solutions (l_k) of the diophantic equation

$$\gamma_0 - \sum_{k=0}^{\infty} l_k z_k^{m-1}(\gamma_0) = 0. \tag{B16}$$

This is possible in some special cases, e.g. for $\gamma_0 = 1$ in class 2. Since $z_n^1(1) = 1$, it follows that Eq. (B16) is satisfied if and only if exactly one entry of (l_k) equals 1 whereas all the others are 0. Adding up all of the weights yields $e^{-2c}\left(\left(2ce^{-2c} - 1\right) e^{2ce^{-2c}} + 1\right)$ as the total weight of $\delta(\gamma - 1)$ from class 2.

The $z^m_{(l_k)}$ have several noteworthy properties most of which are easy to prove by induction over m and are therefore listed below without proof.

1. $z^m_{(l_k)}$ is a rational function of γ with integer coefficients.
2. The degree of the numerator is the same as that of the denominator.
3. The coefficient of the highest power is 1 in both numerator and denominator.
4. $z^m_{(l_k)}$ is a strictly monotonically decreasing function (except at its poles).
5. All roots and poles of $z^m_{(l_k)}$ are located on the non-negative real axis.
6. $z^m_{(l_k)}$ has exactly as many poles as roots. Roots and poles alternate, starting with a root at 0.
7. There are exactly one more roots of $z^m_{(l_k)}$ than there are poles in $\sum_{k=0}^{\infty} l_k z_k^{m-1}$.
8. The sum $\sum_i \left|\frac{\partial z^m_{(l_k)}}{\partial\gamma}(\gamma^m_{(l_k)i})\right|^{-1}$ over all roots $\gamma^m_{(l_k)i}$ of $z^m_{(l_k)}$ equals 1. As stated in the text, this can be proved using Cauchy's integration theorem.

Consider now some $z^m_{(l_k)}$ and choose (l_k) such that only the n-th entry is nonzero. Then we have

$$z^m_{0,\dots,0,l_n,0,\dots} = \frac{\gamma - l_n z_n^{m-1}}{\gamma - 1 - l_n z_n^{m-1}}. \tag{B17}$$

Between two of its poles (see the list of properties above), z_n^{m-1} is a continuous function that maps bijectively onto the real numbers; therefore there exists a $\gamma^m_{l_n}$ in this interval such that $z^m_{(l_k)}(\gamma^m_{l_n}) = 0$. Moreover, when $l_n \to \infty$, the $\gamma^m_{l_n}$ converge to the root $\gamma^{m-1}_{n,i}$ of z_n^{m-1} in this interval. Since z_n^{m-1} is monotonously decreasing, $\gamma^m_{l_n} < \gamma^{m-1}_{n,i}$. This implies that for every peak in the spectrum there are infinitely many other peaks to the left of it in any arbitrarily small interval around this peak. This also applies recursively for each of these satellite peaks! Only the peak at 0 is different: as stated in the list above, all roots of $z^m_{(l_k)}$ are ≥ 0 and thus there are no satellite peaks of $\delta(\gamma)$.

---

[1] J.E. Martin and D. Adolf, Annu. Rev. Phys. Chem. **42**, 311 (1991)
[2] D. Adolf and J.E. Martin, Macromolecules **23**, 3700 (1990)
[3] J.E. Martin, D. Adolf and J.P. Wilcoxon, Phys. Rev. Lett. **22**, 2620 (1988); Phys. Rev. A **39**, 1325 (1989)
[4] D. Durand, M. Delsanti, M. Adam and J.N. Luck, Europhys. Lett. **3**, 297 (1987)
[5] H.H. Winter, Prog. Colloid Polym. Sci. **75**, 104 (1987); F. Chambon and H.H. Winter, Journal of Rheology **31**, 683 (1987); J.C. Scanlan and H.H. Winter, Macromolecules **24**, 47 (1991)
[6] M. Adam, M. Delsanti and D. Durand, Macromolecules **18**, 2285 (1985)
[7] P.M. Goldbart, H.E. Castillo and A. Zippelius, Adv. Phys. **45**, 393 (1996)
[8] A.J. Bray and G.J. Rodgers, Phys. Rev. B **38**, 11461 (1988)
[9] G. Biroli and R. Monasson, J. Phys. A **32**, L255 (1999)
[10] K. Broderix, H. Löwe, P. Müller, and A. Zippelius, Europhys. Lett. **48**, 421 (1999)
[11] P. Grassberger, Physica A **262**, 251 (1999)
[12] D.B. Gingold and C.J. Lobb, Phys. Rev. B **42**, 8220 (1990)
[13] K. Broderix, H. Löwe, P. Müller, and A. Zippelius, preprint. cond-mat/0007088
[14] Broderix K., Goldbart P. M., and Zippelius A. Phys. Rev. Lett **79** (1997), 3688
[15] P. Erdős and A. Rényi, Magyar Tud. Akad. Mat. Kut. Int. Kőzl. **5**, 17 (1960); reprinted in: The Art of Counting edited by J. Spencer (MIT Press, Cambridge, MA) (1973)
[16] I.S. Gradshteyn and I.M. Rhyzik, Table of integrals, series and products (Academic Press, New York) (1980)

[17] K. Mehlhorn and St. Näher, The LEDA Platform of Combinatorial and Geometric Computing, (Cambridge University Press, Cambridge) (1999);
see also http://www.mpi-sb.mpg.de/LEDA/leda.html
[18] D. Stauffer and A. Aharony, Introduction to Percolation Theory, (Taylor and Francis, London) (1994)
[19] B.J.T. Morgan, Elements of Simulation, (Chapman and Hall, London) (1984)
[20] A. Aho, J.E. Hopcroft and J.D. Ullman, The design and analysis of computer algorithms, (Addison-Wesley, Reading, MA) (1974)
[21] W.H. Press, S.A. Teukolsky, W.T. Vetterling, and B.P. Flannery, Numerical Recipes in C, (Cambridge University Press, Cambridge) (1995)
[22] K. Binder and D.W. Heermann, Monte Carlo Simulation in Statistical Physics, (Springer, Heidelberg) (1988)

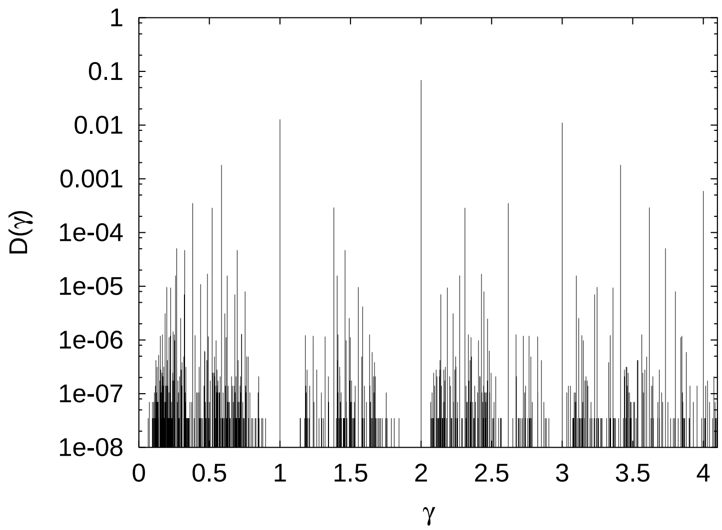

FIG. 1. Numerical simulation of the density of states for $c = 0.1$.

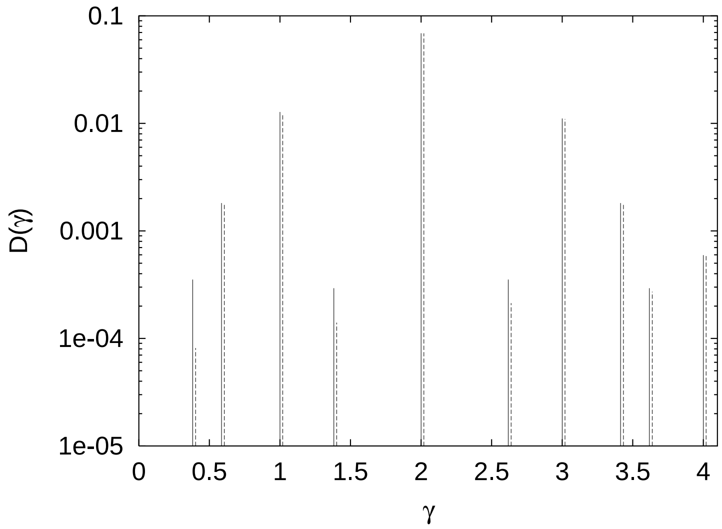

FIG. 2. Comparison between the simulation (solid lines) and some selected peaks calculated from the exact solution (dashed lines) for $c = 0.1$. The analytical peaks have been slightly shifted to the right for better comparison, otherwise they would be indistinguishable from the numerical peaks.

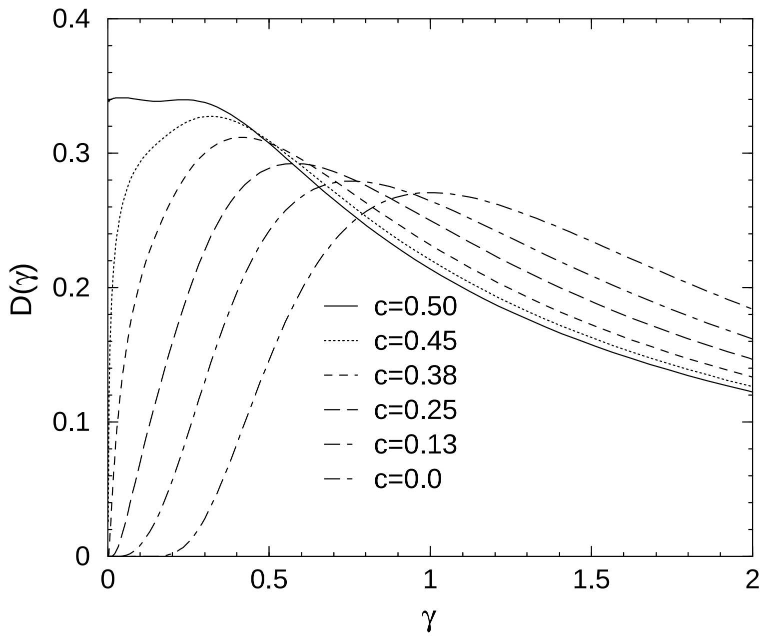

FIG. 3. Density $D(\gamma)$ of non-zero eigenvalues as a function of γ for $p(\lambda)$ given by (70) for several concentrations c. For $c = 0$, the density is given by $D(\gamma) = \frac{1}{2}p(\frac{\gamma}{2})$.

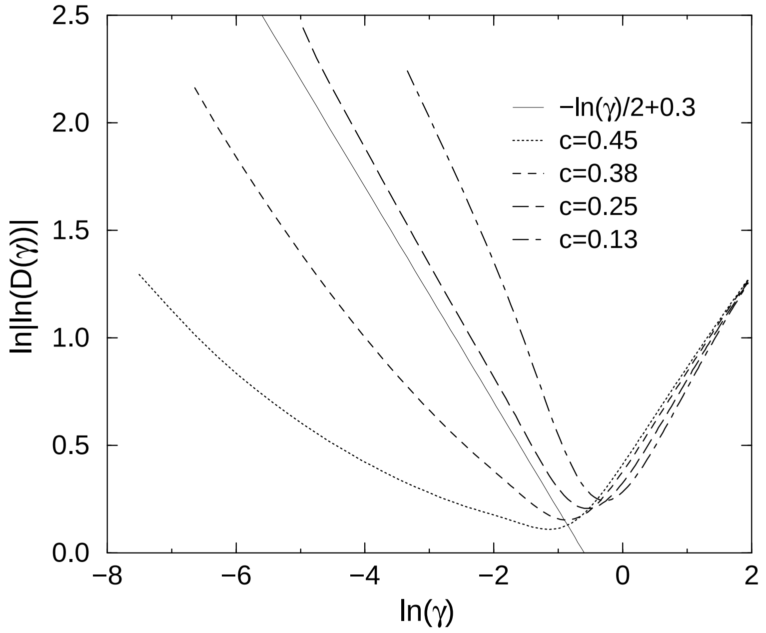

FIG. 4. Double logarithm of the density $D(\gamma)$ of non-zero eigenvalues as a function of $\ln \gamma$ for several concentrations c.

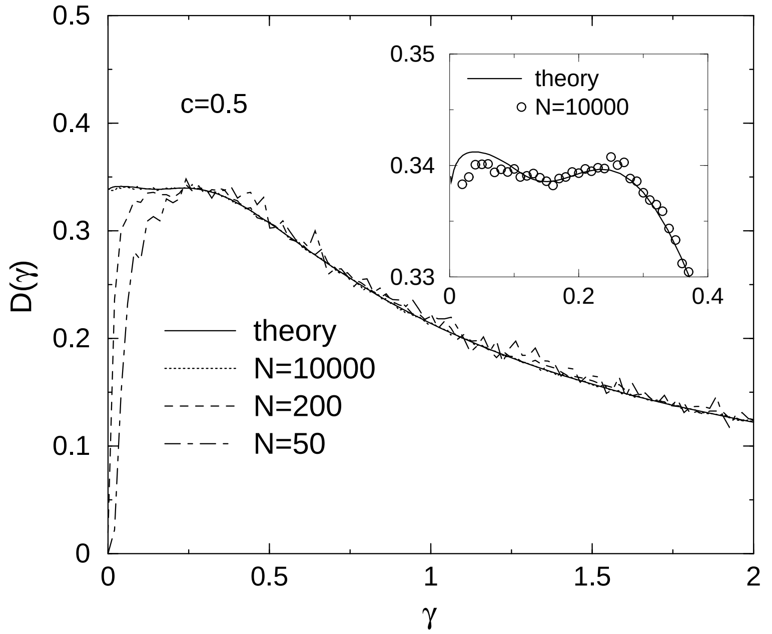

FIG. 5. Density $D(\gamma)$ of non-zero eigenvalues for the mean-field network at the percolation threshold $c = 0.5$ from numerical diagonalization. The solid line is the analytical result, which is hardly distinguishable from the result for $N = 10000$. The inset magnifies the region $\gamma \in [0, 0.4]$, where the numerical results for the largest system size $N = 10000$ are shown by circles.

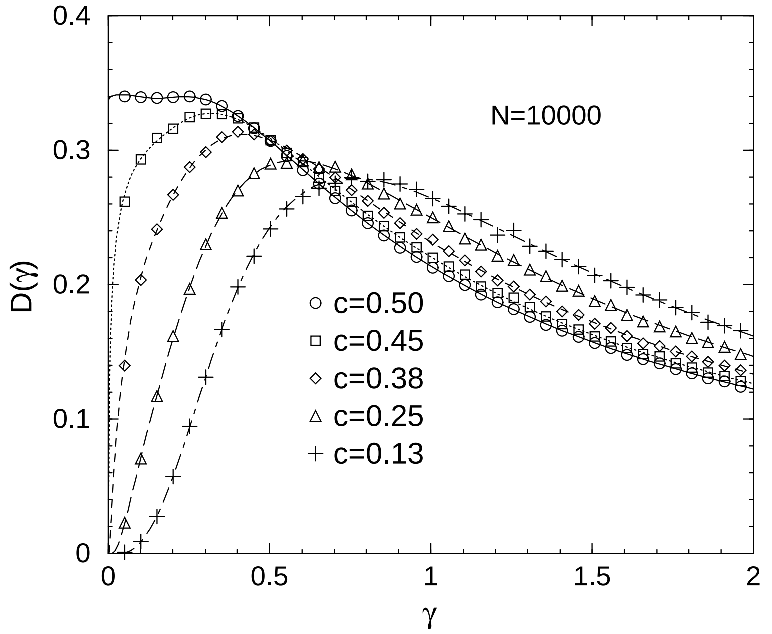

FIG. 6. Density $D(\gamma)$ of non-zero eigenvalues for the mean-field network for different concentrations c. The lines are the analytical results while the numerical data is shown by the symbols.

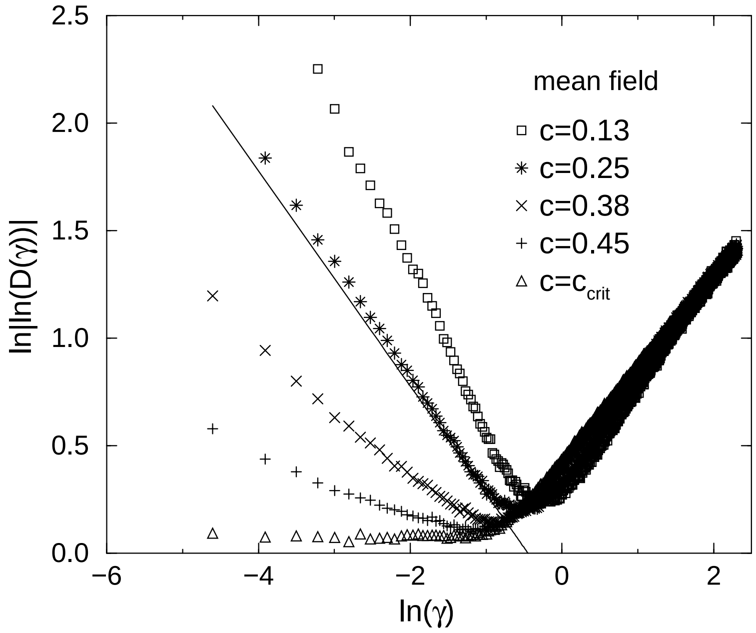

FIG. 7. Double logarithmic plot of $-\ln(D(\gamma))$ for different concentrations c of the mean-field network. The line shows a function $-\ln(\gamma)/2 + const$ (Lifshitz tail), which is the behavior predicted by theory.

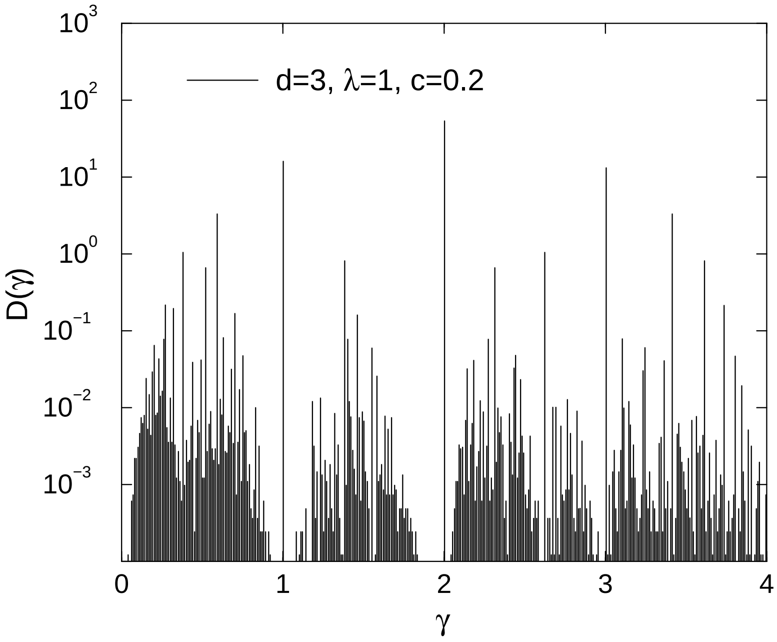

FIG. 8. Density $D(\gamma)$ of non-zero eigenvalues for the cubic network with all bonds having the same strength $\lambda = 1$ ($c = 0.2, N = 16^3$). Similar to the case of the mean-field network, a sum of delta-peaks with strongly varying heights is obtained.

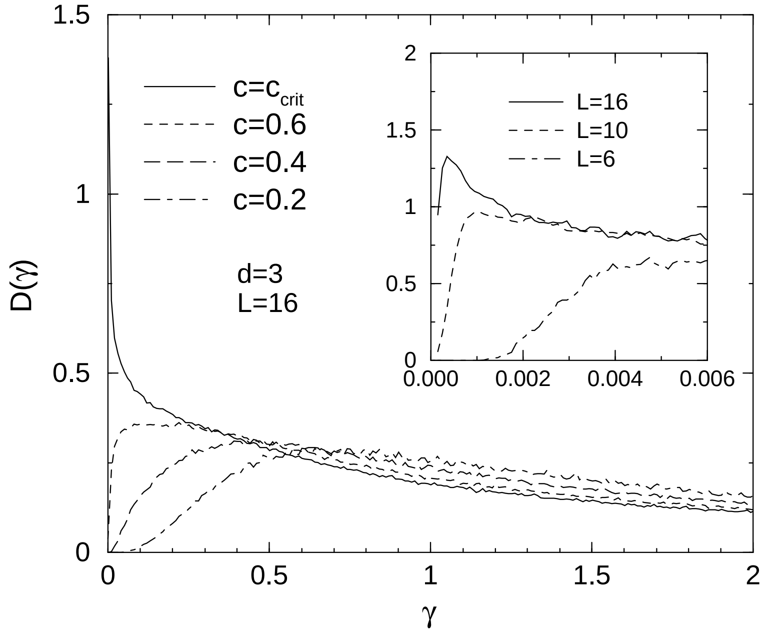

FIG. 9. Density $D(\gamma)$ of non-zero eigenvalues for the cubic network with $p(\lambda)$ given by (70) for different concentrations c. The inset shows the finite-size dependence at the percolation threshold for small eigenvalues.

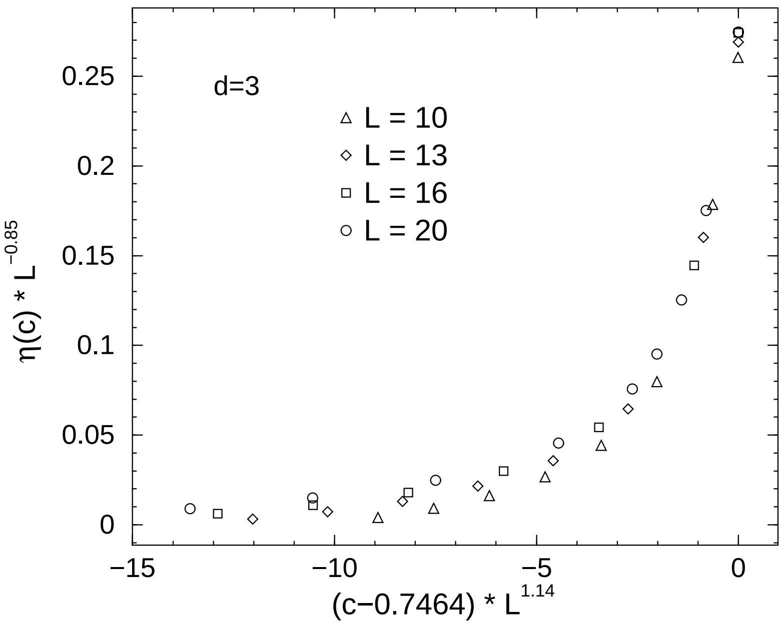

FIG. 10. Finite-size scaling plot of the viscosity $\eta(c, L)$ for the three-dimensional grid. A scaling behavior of $\eta(c, L) = L^{-k/\nu}\tilde{\eta}((c - c_{\mathrm{crit}})L^{1/\nu})$ is assumed. Using $\nu = 0.88$ and $k = 0.75$ the points for $L = 10, 13, 16, 20$ collapse onto one curve near the critical concentration.

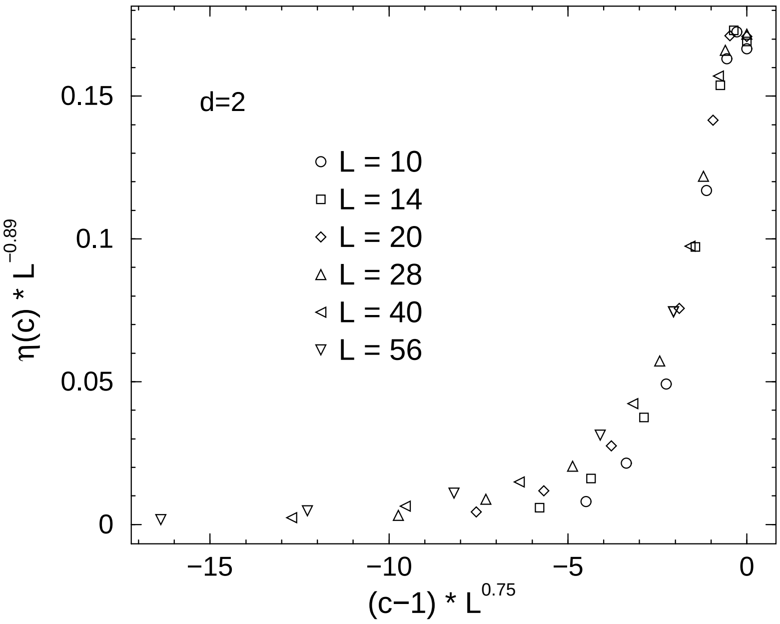

FIG. 11. Finite-size scaling plot of the viscosity $\eta(c, L)$ for the two-dimensional grid. A scaling behavior of $\eta(c, L) = L^{-k/\nu}\tilde{\eta}((c - c_{\rm crit})L^{1/\nu})$ is assumed. Using $\nu = 4/3$ and $k = 1.19$ the points for $L = 10, 14, 20, 28, 40, 56$ collapse onto one curve near the critical concentration. Since finite systems are treated, the maximum of $\eta(c)$ is below the critical concentration $c_{\rm crit} = 1$ of the infinite lattice.

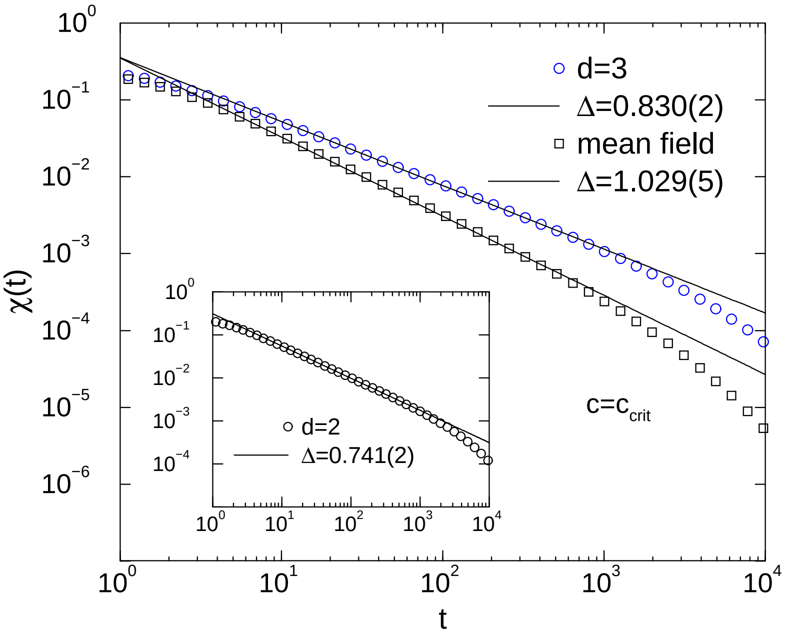

FIG. 12. Stress relaxation function $\chi(t)$ at the the critical concentration $c = c_{\rm crit}$ for the three types of models considered here, with continuously distributed strengths of the crosslinks in all three cases. Shown are the results for the largest sizes which could be treated with sufficient accuracy. For the part of the long-time behavior which is accessible to the numerical simulations, a $\chi(t) \sim t^{-\Delta}$ behavior is visible. From fitting we obtain $\Delta = 1.029$ (mean field), $\Delta = 0.830(2)$ (d=3) and $\Delta = 0.741(2)$ (d=2).

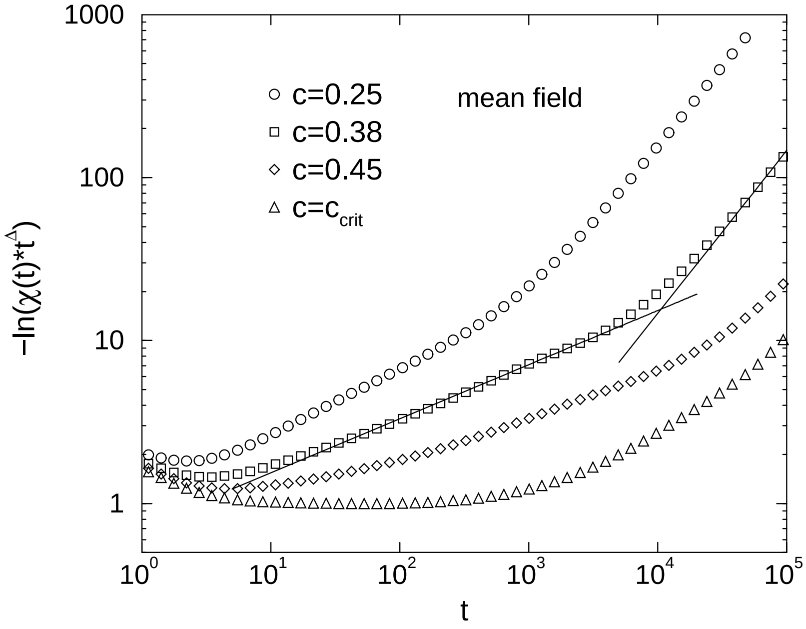

FIG. 13. Rescaled stress relaxation function $-\ln(\chi(t)t^{\Delta})$ as a function of the time for the mean-field network ($\Delta = 1.029$) with different concentrations c of the crosslinks. The straight lines correspond to stretched exponentials with exponent $\beta = 0.332$ and $\beta = 1$.

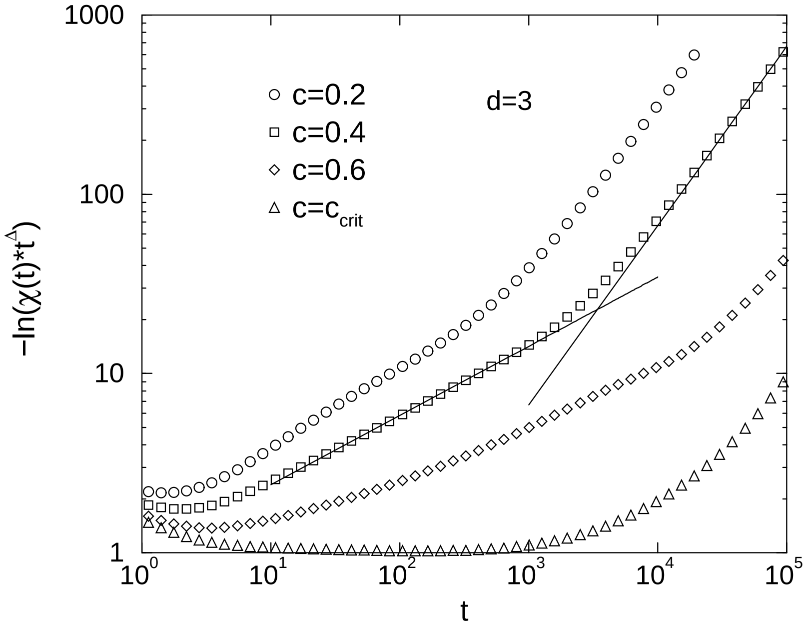

FIG. 14. Rescaled stress relaxation function $-\ln(\chi(t)t^{\Delta})$ as a function of the time for the three-dimensional network ($\Delta = 0.830$) with different concentrations c of the crosslinks. The straight lines correspond to stretched exponentials with exponent $\beta = 0.386$ and $\beta = 1$.

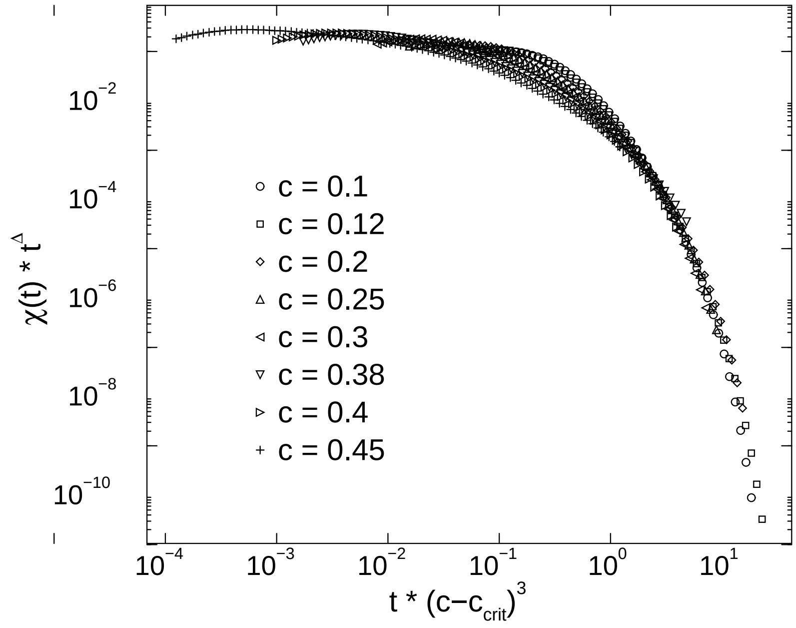

FIG. 15. Scaling plot for the stress relaxation $\chi(t)t^{\Delta}$ as a function of $t(c_{\rm crit} - c)^z$ for the mean-field network ($N = 10^4$, randomly distributed strengths of crosslinks) with the values $\Delta = 1, z = 3$.